U. S. DEPARTMENT OF COMMERCE
NATIONAL OCEANIC AND ATMOSPHERIC ADMINISTRATION
NATIONAL WEATHER SERVICE
NATIONAL METEOROLOGICAL CENTER

OFFICE NOTE 163

Real Data Experimentation with Higher Order Finite
Differencing in the Semi-Implicit Version of the Shuman-Hovermale Model

K. A. Campana
Development Division

November 1977

Real Data Experiments with Higher-Order Finite Differencing
in the Semi-Implicit Version of the Shuman Hovermale Model

1. Introduction

In grid point numerical models of the atmosphere, truncation errors
in space[1] result from using finite-difference approximations to the
appropriate set of continuous equations. These errors usually appear as
a retardation of forecasted phase speeds of meteorological features.
There are several techniques available to reduce this truncation error.

One method is to use finer resolution models. The smaller grid point
separation means that the model finite differences will be closer approxi-
mations to the continuous equations. During finer mesh forecasts, this
will show up as "better" translational speeds of the meteorological
features. Of course, the finer grid also will be able to resolve small-
scale features that the coarse grid "cannot see." These features may
have a significant impact on model forecasts. However, the use of fine-
mesh models is quite expensive computationally. In order to cover the
same geographical area as a coarse grid model, the finer mesh requires
more grid points and a shorter time step. A doubling of the horizontal
resolution increases the number of grid points by a factor of 4 while
requiring a reduction in the time step by one-half.

An alternative method of reducing truncation error is to use more
accurate finite-difference approximations to the equations without
reducing the grid spacing. Here at NMC, Gerrity, McPherson, and Polger
(1972) have shown that more accurate finite-differencing for Shuman's
(1962) semimomentum form of the advective terms will reduce truncation
error in the longer waves and result in increased phase speeds for these
meteorological features. Their method is quite efficient since there is
no increase in the number of grid points; however, the time step length
must be reduced by approximately 30% of its normal value.

Often the major difference between NMC's 6-layer primitive equation
model (6L PE) and its finer mesh offspring, the LFM, is the speed at
which features move during a forecast. More accurate finite differencing,
using the second method above, would make the 6L PE competitive with the
LFM in these cases--at a much smaller cost in resources. Of course, in
situations where finer resolution is needed to portray the evolution of
important small-scale features, the LFM probably would be superior.

The purpose of this note is to discuss several real data experiments
using a model containing more accurate finite differences in the advective
terms of the equations. The semi-implicit model developed by Gerrity,

---

[1]Time truncation errors are not discussed in this report.

McPherson, and Scolnik (1973) and subsequently discussed by Campana (1974, 1977) is chosen for these tests. It is a model patterned after the 6L PE and thus has a grid spacing of 381 kilometers at 60°N on a polar stereographic projection of the Northern Hemisphere. It contains all the physical parameterizations of the 6L PE, but unlike the 6L PE it staggers the wind components (u,v) with respect to the other variables on the horizontal grid--the wind components being located in the center of grid boxes and all other variables being found at grid points. Of course, the long time step permitted by the semi-implicit technique makes the model an efficient research tool.

The next section in this note will describe the finite-differencing used by the model in considerable detail. The third section will present the results of three test forecasts in situations where the 6L PE had particular difficulty. Comparisons will be made between "normal" semi-implicit forecasts and those using the more accurate finite-differencing. These results also will be compared with the higher-resolution version of the 6L PE (which has used the same initial data as the semi-implicit model).

2. Finite Differencing

This section presents the form of the model finite differences that are used in the real data experiments. Much of the material is obtained from papers by Gerrity, McPherson, and Polger (1972) and Gerrity (1973). These papers develop the more accurate finite difference scheme in Shuman's (1962) semimomentum form. The author will reproduce from these papers some of the steps involved in obtaining the two-dimensional semimomentum form of the first derivative. This background is then used to show the grid points that are part of the first derivative in both the normal finite-difference form and its more accurate counterpart.

First consider one-dimension. The Taylor series representation of a function, f(x), in some neighborhood of a grid point, x_i, is =

$$f\left(x_i + \frac{\Delta x}{2}\right) = f(x_i) + \frac{\partial f}{\partial x}\frac{\Delta x}{2} + \frac{1}{2!}\frac{\partial^2 f}{\partial x^2}\left(\frac{\Delta x}{2}\right)^2 + \frac{1}{3!}\frac{\partial^3 f}{\partial x^3}\left(\frac{\Delta x}{2}\right)^3 + 0\left[\left(\frac{\Delta x}{2}\right)^4\right] \quad (1)$$

Similarly for $f\left(x_i - \frac{\Delta x}{2}\right)$ one obtains:

$$f\left(x - \frac{\Delta x}{2}\right) = f(x_i) - \frac{\partial f}{\partial x}\frac{\Delta x}{2} + \frac{1}{2!}\frac{\partial^2 f}{\partial x^2}\left(\frac{\Delta x}{2}\right)^2 - \frac{1}{3!}\frac{\partial^3 f}{\partial x^3}\left(\frac{\Delta x}{2}\right)^3 + 0\left[\left(\frac{\Delta x}{2}\right)^4\right] \quad (2)$$

where $O[(\Delta x/2)^4]$ represents neglected terms, Δx is the grid spacing, and $\Delta x/2$ is used to obtain the Shuman semimomentum form. The power of $\Delta x/2$ in the right-most term of eqs (1) and (2) refers to the leading neglected term. Subtracting eq (2) from eq (1) and dividing by Δx one obtains the following Taylor series representation of the first derivative:

$$\frac{\partial f}{\partial x} = \frac{f(x_i + \Delta x/2) - f(x_i - \Delta x/2)}{\Delta x} - \frac{1}{3!}\frac{\partial^3 f}{\partial x^3}\left(\frac{\Delta x}{2}\right)^2 - O\left[\left(\frac{\Delta x}{2}\right)^4\right] \qquad (3)$$

The order of the finite difference is defined as the exponent of Δx contained in the leading term of those neglected. The fourth-order form is shown in eq (3) and is the one being tested. The first term on the right side of eq (3) is Shuman's "normal" second-order accurate (in space) centered difference form of the first derivative. Both the second and fourth-order accurate finite-difference forms of the first derivative are discussed next.

Recall that Shuman's second-order form of the derivative is computed midway between grid points. It is transferred back to grid points by an averaging scheme. The symbolic operators for the derivative, f_x, and the averaging, $\bar{f}^x$, are defined below:

$$f_x = \frac{1}{\Delta x}\left(f_{i+\frac{1}{2}} - f_{i-\frac{1}{2}}\right) \qquad (4)$$

$$\bar{f}^x = \frac{1}{2}\left(f_{i+\frac{1}{2}} + f_{i-\frac{1}{2}}\right) \qquad (5)$$

where integer values of i refer to grid points in the x direction ($i\pm\frac{1}{2}$ referring to positions midway between grid points).

In developing the fourth-order accurate derivative, the $\partial^3 f/\partial x^3$ term in eq (3), is evaluated such that it is valid at the same grid location as f_x. Using eq (4), the second derivative, f_{xx}, and the third derivative, f_{xxx}, become

$$f_{xx} = \frac{1}{(\Delta x)^2}\left(f_{i+1} - 2f_i + f_{i-1}\right) \qquad (6)$$

$$f_{xxx} = \frac{1}{(\Delta x)^3}\left(f_{i+3/2} - f_{i-3/2} - 3f_{i+\frac{1}{2}} + 3f_{i-\frac{1}{2}}\right) \qquad (7)$$

Inserting eq (7) into eq (3) one obtains the fourth-order approximation for the derivative, f_{x_h}:

$$f_{x_h} = \frac{9}{8}\left(\frac{f_{i+\frac{1}{2}} - f_{i-\frac{1}{2}}}{\Delta x}\right) - \frac{1}{8}\left(\frac{f_{i+3/2} - f_{i-3/2}}{3\Delta x}\right) \tag{8}$$

where the subscript, h, denotes the higher-order scheme. From Gerrity et al. (1972) the companion averaging $\bar{f}^{x_h}$ is:

$$\bar{f}^{x_h} = \frac{9}{8}\left(\frac{f_{i+\frac{1}{2}} + f_{i-\frac{1}{2}}}{2}\right) - \frac{1}{8}\left(\frac{f_{i+3/2} + f_{i-3/2}}{2}\right) \tag{9}$$

As in the second-order form, the derivative is valid midway between grid points and the averaging operator is used to bring it back to the points. The combined operator, derivative and averaging, is represented symbolically as $\bar{f}_x^x$ for the second-order scheme and as $\bar{f}_{x_h}^{x_h}$ for the fourth order.

In two dimensions (x,y) the derivatives are calculated in the center of grid boxes by using a difference in one direction and an average in the other ($\bar{f}_x^y$ or $\bar{f}_y^x$). The derivative is returned to grid points by an averaging process, $\bar{f}^{xy}$. By combining eqs (4, 5) one obtains the following second-order forms for Shuman's finite differences--both derivatives and averaging:

$$\bar{f}_x^y = \frac{1}{2\Delta x}\left(f_{i+\frac{1}{2},j+\frac{1}{2}} - f_{i-\frac{1}{2},j+\frac{1}{2}} + f_{i+\frac{1}{2},j-\frac{1}{2}} - f_{i-\frac{1}{2},j-\frac{1}{2}}\right) \tag{10}$$

$$\bar{f}_y^x = \frac{1}{2\Delta x}\left(f_{i+\frac{1}{2},j+\frac{1}{2}} - f_{i+\frac{1}{2},j-\frac{1}{2}} + f_{i-\frac{1}{2},j+\frac{1}{2}} - f_{i-\frac{1}{2},j-\frac{1}{2}}\right) \tag{11}$$

$$\bar{f}^{xy} = \frac{1}{4}\left(f_{i+\frac{1}{2},j+\frac{1}{2}} + f_{i+\frac{1}{2},j-\frac{1}{2}} + f_{i-\frac{1}{2},j-\frac{1}{2}} + f_{i-\frac{1}{2},j+\frac{1}{2}}\right) \tag{12}$$

where integer values of j refer to grid points in the y-direction.

Using a similar process, eqs (8,9) are combined to produce the following two-dimensional fourth-order finite-difference forms:

$$\overline{f}_{x_h}^{y_h} = \frac{1}{384\Delta x}[243\left(f_{i+\frac{1}{2},j+\frac{1}{2}} - f_{i-\frac{1}{2},j+\frac{1}{2}} + f_{i+\frac{1}{2},j-\frac{1}{2}} - f_{i-\frac{1}{2},j-\frac{1}{2}}\right)$$

$$- 27\left(f_{i+\frac{1}{2},j+3/2} - f_{i-\frac{1}{2},j+3/2} + f_{i+\frac{1}{2},j-3/2} - f_{i-\frac{1}{2},j-3/2}\right)$$

$$- 9\left(f_{i+3/2,j+\frac{1}{2}} - f_{i-3/2,j+\frac{1}{2}} + f_{i+3/2,j-\frac{1}{2}} - f_{i-3/2,j-\frac{1}{2}}\right) \quad (13)$$

$$+ \left(f_{i+3/2,j+3/2} - f_{i-3/2,j+3/2} + f_{i+3/2,j-3/2} - f_{i-3/2,j-3/2}\right)]$$

$$\overline{f}_{y_h}^{x_h} = \frac{1}{384\Delta x}[243\left(f_{i+\frac{1}{2},j+\frac{1}{2}} - f_{i+\frac{1}{2},j-\frac{1}{2}} + f_{i-\frac{1}{2},j+\frac{1}{2}} - f_{i-\frac{1}{2},j-\frac{1}{2}}\right)$$

$$- 27\left(f_{i+3/2,j+\frac{1}{2}} - f_{i+3/2,j-\frac{1}{2}} + f_{i-3/2,j+\frac{1}{2}} - f_{i-3/2,j-\frac{1}{2}}\right)$$

$$- 9\left(f_{i+\frac{1}{2},j+3/2} - f_{i+\frac{1}{2},j-3/2} + f_{i-\frac{1}{2},j+3/2} - f_{i-\frac{1}{2},j-3/2}\right) \quad (14)$$

$$+ \left(f_{i+3/2,j+3/2} - f_{i+3/2,j-3/2} + f_{i-3/2,j+3/2} - f_{i-3/2,j-3/2}\right)]$$

and

$$\overline{f}^{x_h y_h} = \frac{1}{256}[81\left(f_{i+\frac{1}{2},j+\frac{1}{2}} + f_{i+\frac{1}{2},j-\frac{1}{2}} + f_{i-\frac{1}{2},j+\frac{1}{2}} + f_{i-\frac{1}{2},j-\frac{1}{2}}\right)$$

$$- 9\left(f_{i+3/2,j+\frac{1}{2}} + f_{i+3/2,j-\frac{1}{2}} + f_{i-3/2,j+\frac{1}{2}} + f_{i-3/2,j-\frac{1}{2}}\right.$$

$$\left. + f_{i+\frac{1}{2},j+3/2} + f_{i+\frac{1}{2},j-3/2} + f_{i-\frac{1}{2},j+3/2} + f_{i-\frac{1}{2},j-3/2}\right) \quad (15)$$

$$+ \left(f_{i+3/2,j+3/2} + f_{i+3/2,j-3/2} + f_{i-3/2,j+3/2} + f_{i-3/2,j-3/2}\right)]$$

As is evident from eqs (13-15) the fourth-order scheme requires a great deal more computation than the second-order forms in eqs (10-12). Also the higher-order scheme requires four grid rows in central memory of the computer.

In the tests shown in the next section, fourth-order finite differences are applied to the horizontal advection terms in each equation. Since the semi-implicit model has u,v wind components staggered (in grid boxes) with respect to the other variables, their finite difference forms will be somewhat different than the other variables. For the u,v equations, the advection terms are symbolically represented as:

$$u\frac{\partial u}{\partial x} + v\frac{\partial u}{\partial y} \;\rightarrow\; \left(\overline{u}^{x_h y_h}\; \overline{u_{x_h}}^{y_h} + \overline{v}^{x_h y_h}\; \overline{u_{y_h}}^{x_h} \right)^{x_h y_h} \tag{16}$$

For grid point variables (T for temperature):

$$u\frac{\partial T}{\partial x} + v\frac{\partial T}{\partial y} \;\rightarrow\; \left(u\; \overline{T_{x_h}}^{y_h} + v\; \overline{T_{y_h}}^{x_h} \right)^{x_h y_h} \tag{17}$$

3. Test Results

In the tests presented here, parallel experiments have been made with a second-order semi-implicit model (S2) and a fourth-order version (S4). The models are identical except for the finite-difference form of the advection terms. The increased computation time resulting from using eqs (13-15) in the S4 model rather than eqs (10-12) amounts to about 10%. Additionally a 25% reduction in time step has been used with the S4 model--a 30-minute step rather than the 40-minute one in the S2 model.

Two well known NMC model forecast problems are tackled in the real data experiments. They are the "locked-in" and "cross-contour flow" situations. "Locked-in" refers to the tendency of the forecast model to predict 500-mb heights much too high over a vigorously developing storm and much too low behind and to the south. "Cross-contour" refers to the tendency of the forecast model to predict strong maximum winds that appear to flow across the isobars from low pressure to high pressure--usually above 500 mb. Tests with a higher resolution version of the 6L PE (HFM)[2] have produced more accurate forecasts than the 6L PE in these cases. The apparent relation of space truncation error to the "locked-in" and "cross-contour" problems means they are excellent cases for testing the fourth-order model.

---

[2]Hemispheric Fine Mesh

The first case (9 Jan 00Z) is one in which the 6L PE became badly "locked-in" by 48 hours. Figs. 1 and 2 show the 24-hr surface and 500-mb forecasts of the S2 and S4 models. Also included are the verifying analyses. Even as early as 24 hours the higher-order scheme is moving the 500-mb trough and vorticity through Texas at a faster, more accurate speed. Both models miss the intensity of the vorticity maximum in North Dakota and the finger of positive vorticity pointing at Ohio. Figures 3 and 4 contain similar maps for 48 hours. The S4 model produces an excellent forecast. Its surface low is further north and looks more occluded than in the S2 model. The location of the low too far into the cold air could be explained if the model failed to predict the coastal development that occurred in the "real" atmosphere about 12 hours earlier. At 500 mb the vorticity maximum over West Virginia is quite close to the observed location. The 48-hr 500-mb height error (meters) for both models is shown in Fig. 5. The typical "locked-in" error pattern for the S2 model has been significantly reduced by the S4 model.

For comparison the 48-hr forecasts made by the HFM and 6L PE models are shown in Fig. 6. The HFM makes improvements to its coarse mesh counterpart in much the same manner as the S4 does to its second-order brother, the S2 model. The use of staggered variables in the semi-implicit model has contributed to the S2 model's superiority over the 6L PE, but both models still suffer from the "locked-in" problem. The S4 model is easily superior to the HFM in this case.

Maps of 12-hr accumulated precipitation (inches) ending at 48 hours for the various models are shown in Fig. 7, and the verifying chart is shown in Fig. 8. The S4 model has improved the precipitation forecast of the S2 model even though both maxima are over New York City and slow. In the S4 version, the southern finger of maximum precipitation is swung more correctly to the Carolina coast. The forecast of larger amounts north of Lakes Ontario and Erie is also more correct, but may be a result of over-forecasting.

The second case uses data from 12Z 9 January 1975 and is another "locked-in" situation. Figs. 9, 10, and 11 show the 48-hr forecasts of the S2 and S4 models and the verifying analyses for sea level, 500 mb and 300 mb. Comparable HFM forecasts are included in the figures. Fig. 12 shows the 48-hr 500-mb height error (meters) for both the S4 and S2 models. Again the "locked-in" error is apparent in the S2 model. The error has been halved in the northern United States by the S4 model, but it only has moved further northeastward in the southern United States. At the surface, unlike the other models, S4 shows an apparent frontal trough through the Virginias and Carolinas which verifies quite well. The overall S4 forecast is quite similar to that of the HFM, even though its 500-mb trough is deeper over the southeastern United

States. Though the 6L PE forecasts are not presented, the HFM improvement over the 6L PE again is much the same as the S4 superiority over the S2.

The 12-hr accumulated precipitation forecasts for this case are shown in Fig. 13 and the verification is found in Fig. 14. The S4 model forecast is quite remarkable in the southeastern United States where a front is again implied. There also appears to be a rudimentary "dry tongue" in Tennessee, which may show the S4 model's ability to more accurately portray the storm occlusion process.

The third test case uses initial data from 00Z 17 February 1977 and is one in which the 36-hr 6L PE forecast contains severe cross-contour flow near Hawaii. Comparisons between the 36-hr 300-mb forecasts for the S2 and S4 models are shown in Fig. 15, and for the 6L PE and HFM models in Fig. 16. The verifying analysis appears in Fig. 17. The S4 model has removed the cross-contour flow in much the same manner as the HFM.

4. Conclusion

Two methods of reducing truncation error in space have been tried in NMC numerical models. One is to reduce the spacing between grid points. The other is to employ more accurate finite-differencing schemes for the advective processes without reducing grid spacing. In forecast situations where space truncation error seems to be important (locked-in and cross-contour flow), both methods produce similar improvements over the original model. While the fine mesh probably is superior, since it can resolve potentially important small-scale features, more accurate finite differencing is able to achieve comparable forecast improvements in larger-scale features—and at a less expensive computational cost.

REFERENCES

Campana, K. A., "Status report on a semi-implicit version of the Shuman-Hovermale model," NOAA Technical Memorandum NWS-NMC 54, 1974, 22 pp.

_____ "Addition of orography to the semi-implicit version of the Shuman-Hovermale model," NMC Office Note 153, 1977, 9 pp.

_____ "Semi-implicit higher order version of the Shuman-Hovermale model," to be published as a NOAA Technical Memorandum.

Gerrity, J. P., "Numerical advection experiments with higher order accurate semimomentum approximations," Monthly Weather Review, 101, 1973, pp. 231-234.

_____, R. D. McPherson, and P. D. Polger, "On the efficient reduction of truncation error in numerical weather prediction models," Monthly Weather Review, 100, 1972, pp. 637-643.

_____, and S. H. Scolnik, "A semi-implicit version of the Shuman-Hovermale model," NOAA Technical Memorandum NWS-NMC 53, 1973, 44 pp.

Shuman, F. G., "Numerical experiments with the primitive equations," Proceedings of the International Symposium on Numerical Weather Prediction, Tokyo, Japan, November 7-13, 1960, Meteorological Society of Japan, March 1962, pp. 85-107.
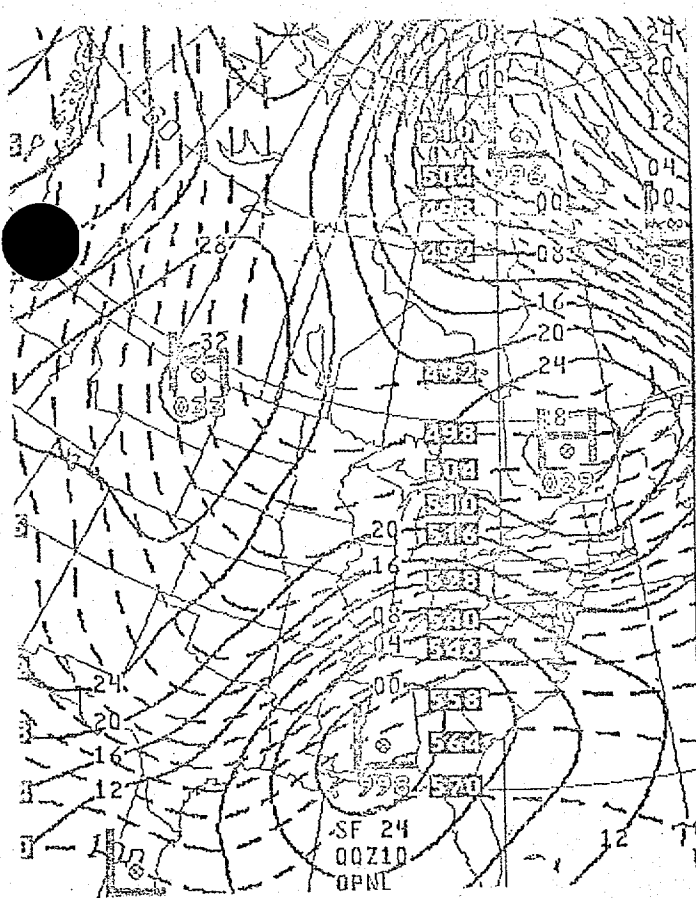
S4
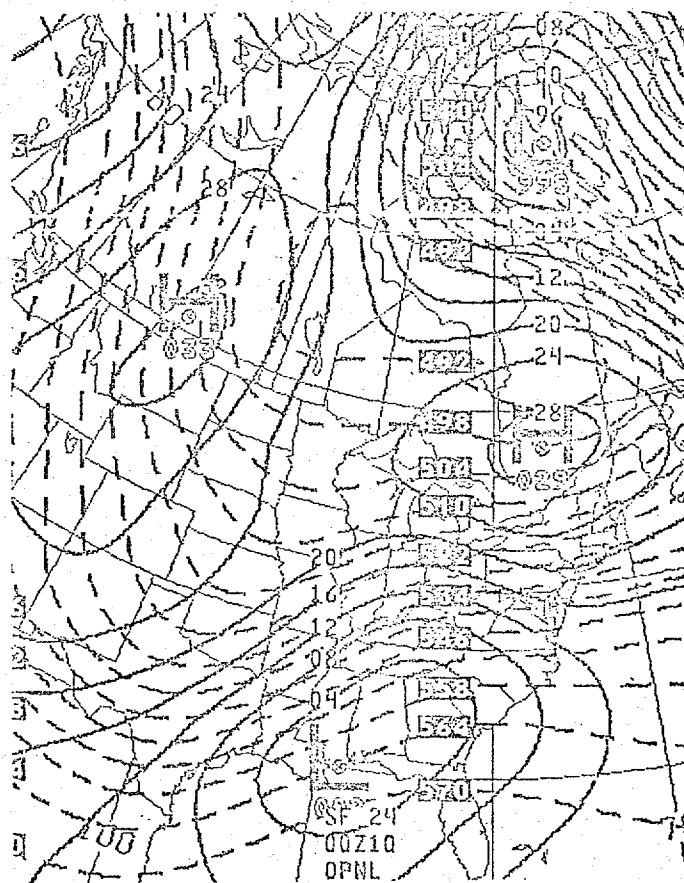
S2

24HR FCST

SFC/1000-500 THICKNESS VALID 00Z MON 10 JAN 1977
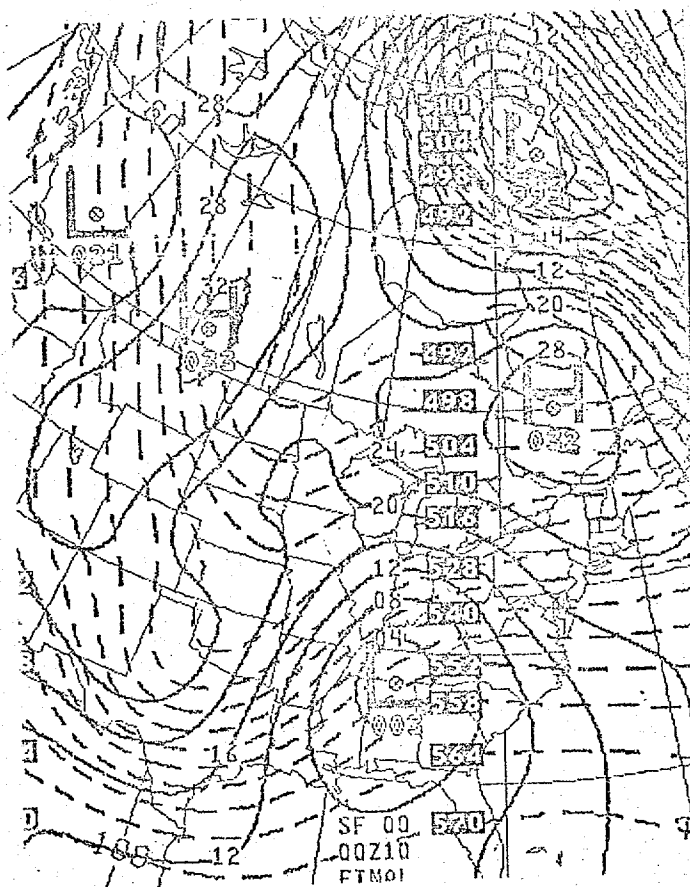
VERIFICATION

Figure 1
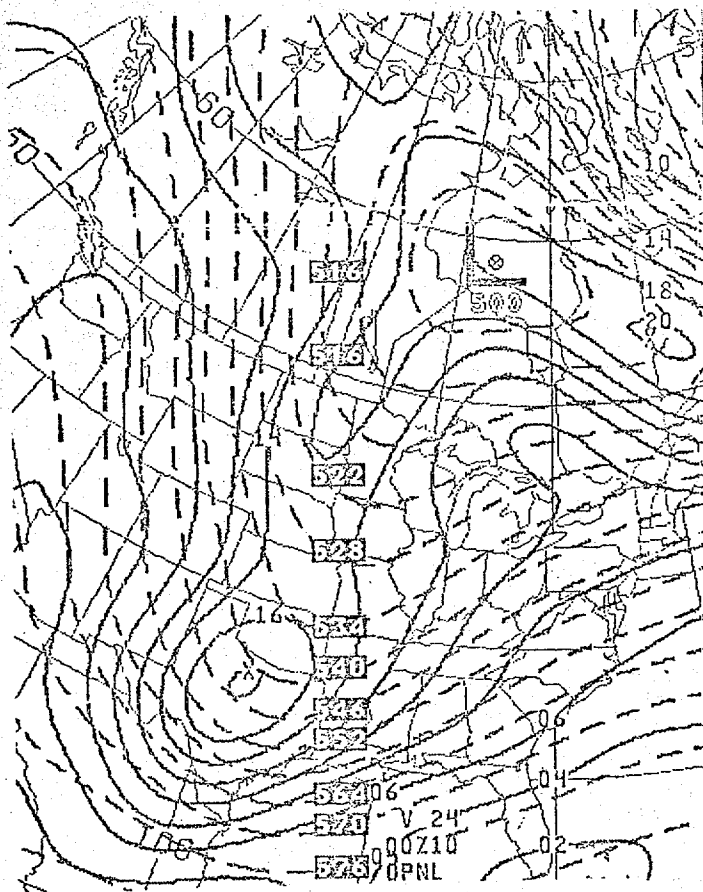
S4
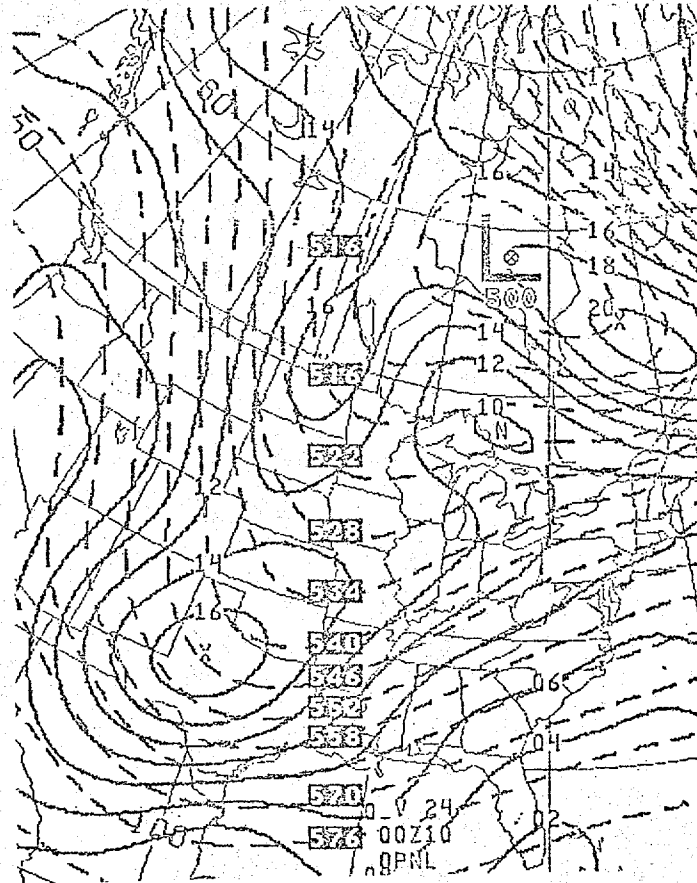
S2

24HR FCST 500MB HEIGHTS/VORTICITY VALID 00Z MON 10 JAN 1977
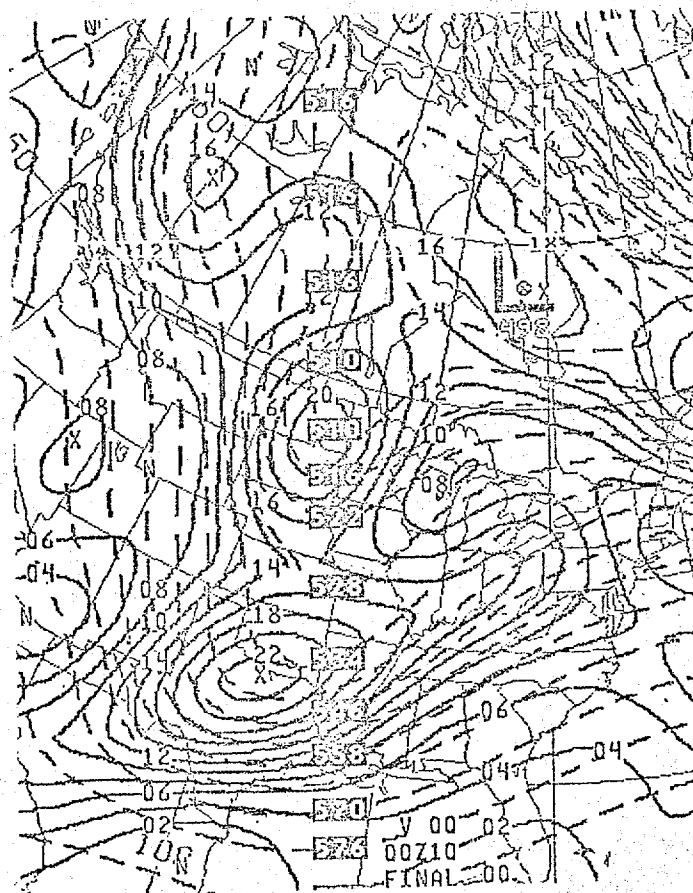
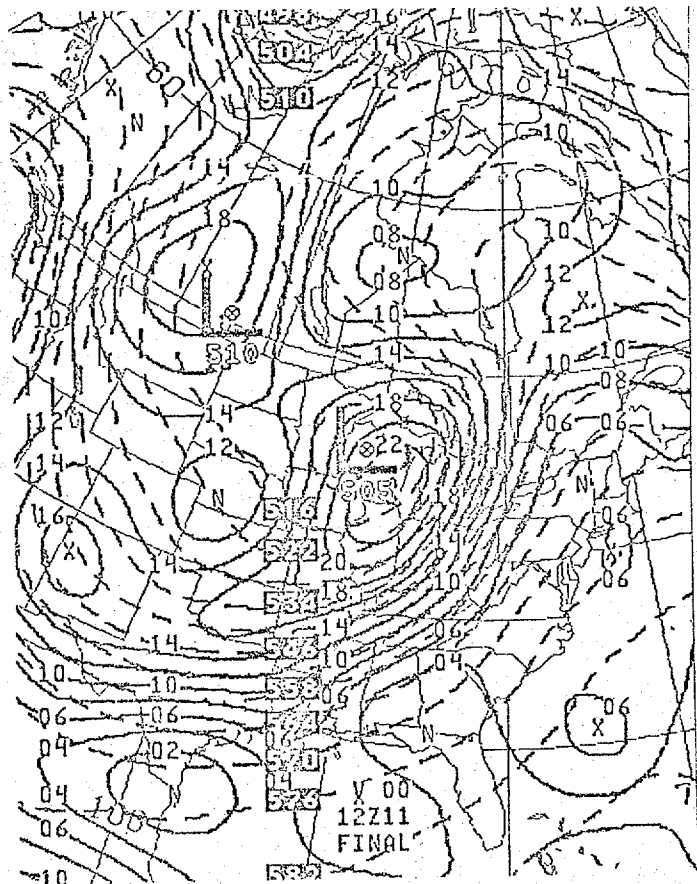VERIFICATION

Figure 2

S4

S2

48HR' FCST   SFC/1000-500 THICKNESS VALID 00Z TUE 11 JAN 1977
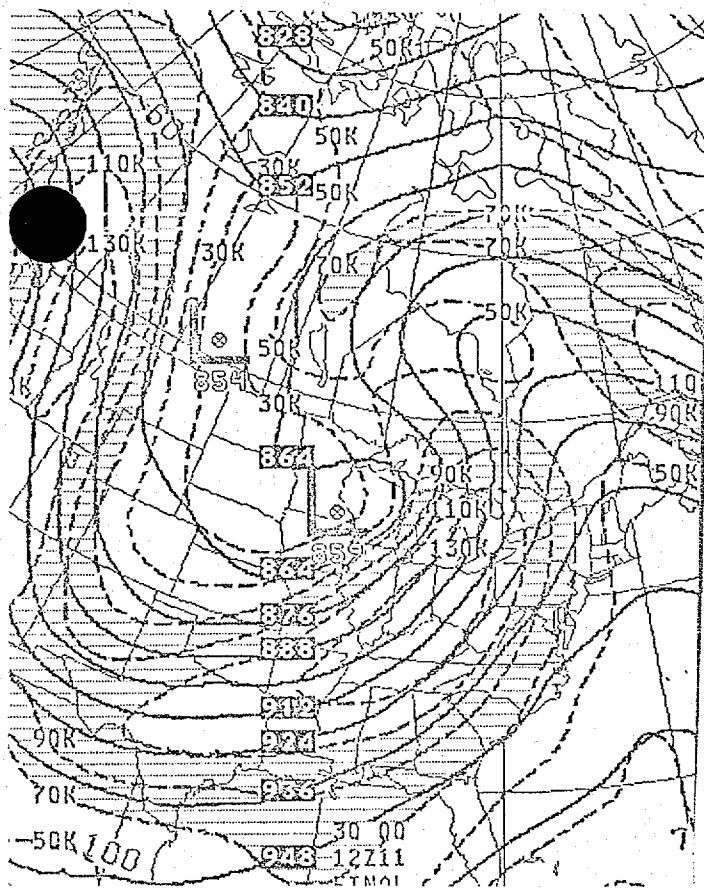
VERIFICATION
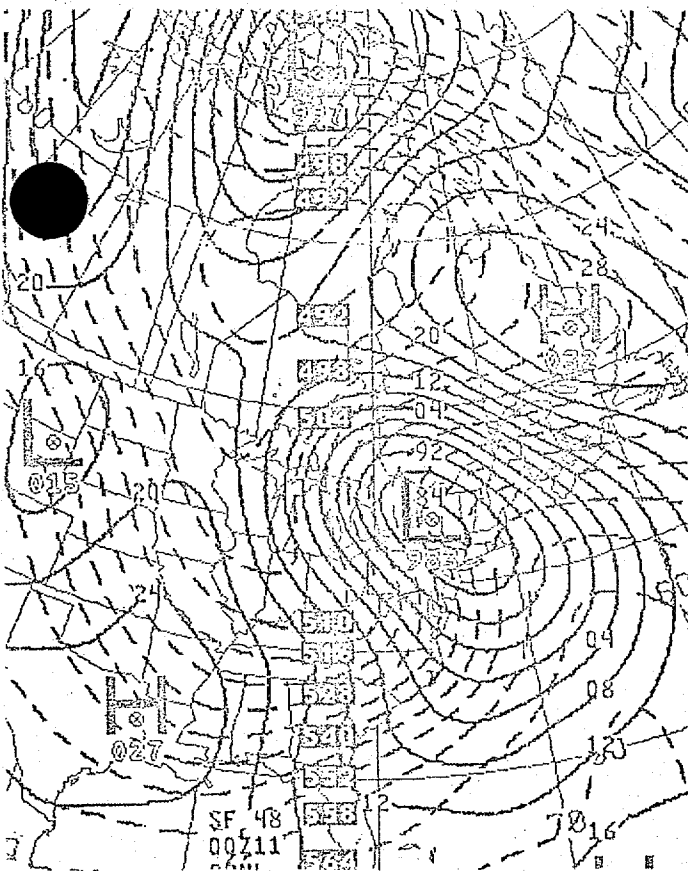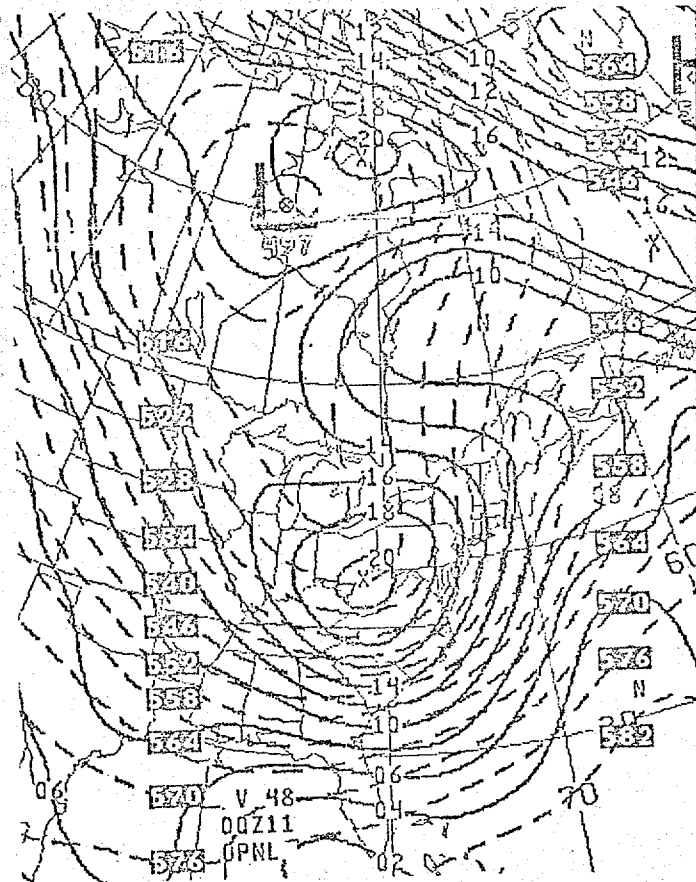
Figure 3

S4

S2
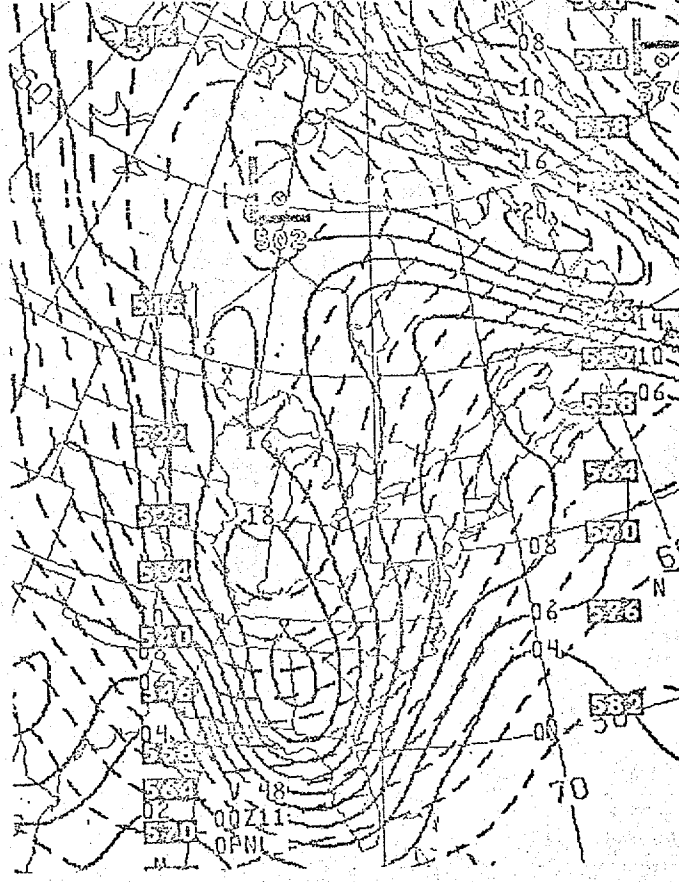
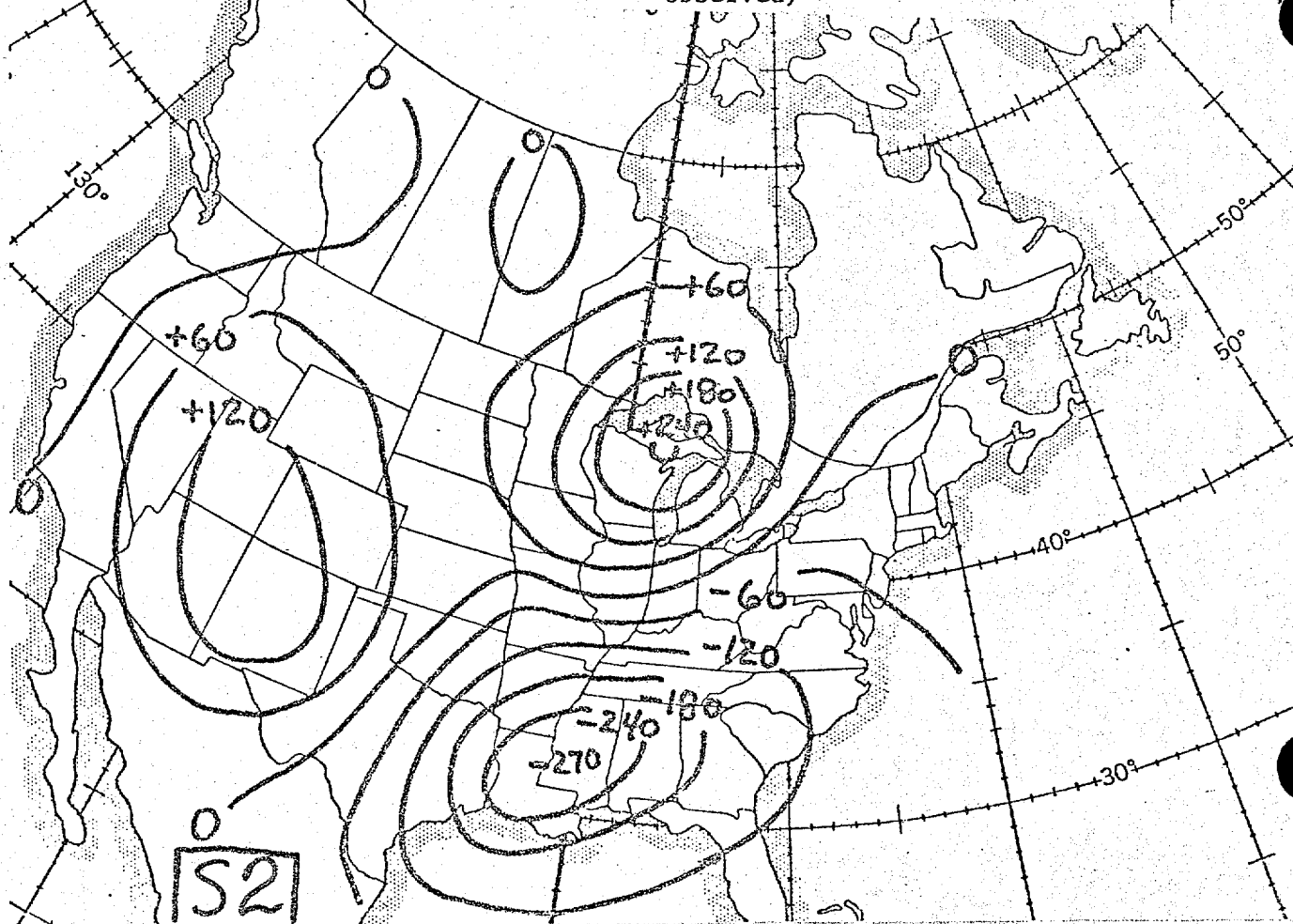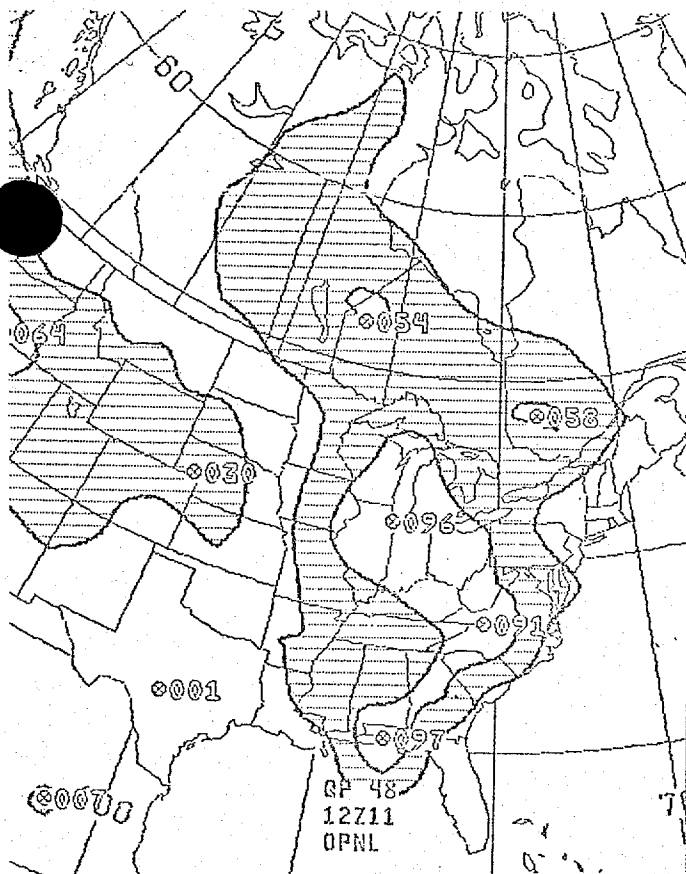48HR FCST 500MB   HEIGHTS/VORTICITY   VALID 00Z TUE 11 JAN 1977
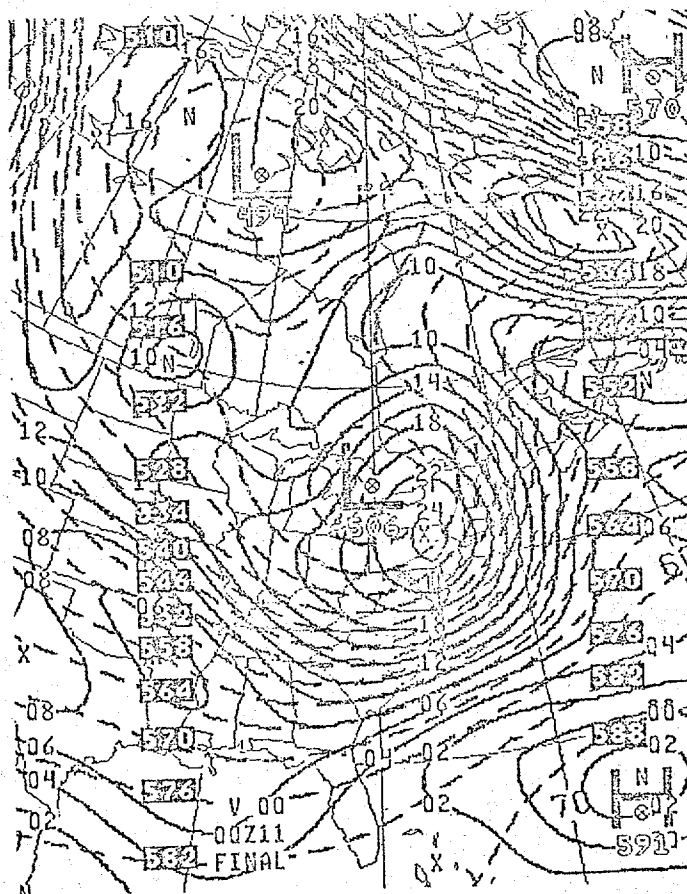
VERIFICATION

Figure 4
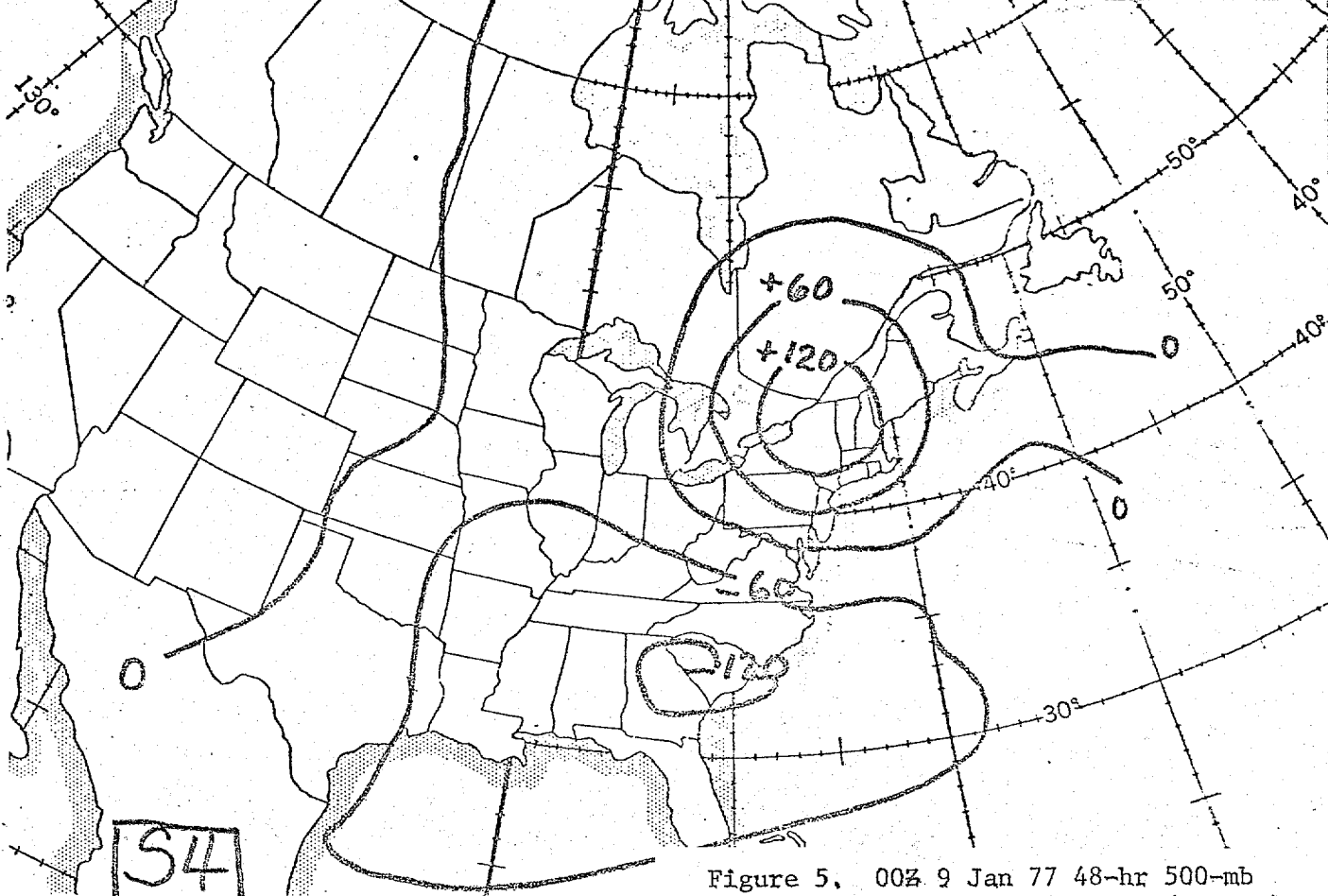
Figure 5. 00Z 9 Jan 77 48-hr 500-mb
height differences (meters)
(forecast-observed)
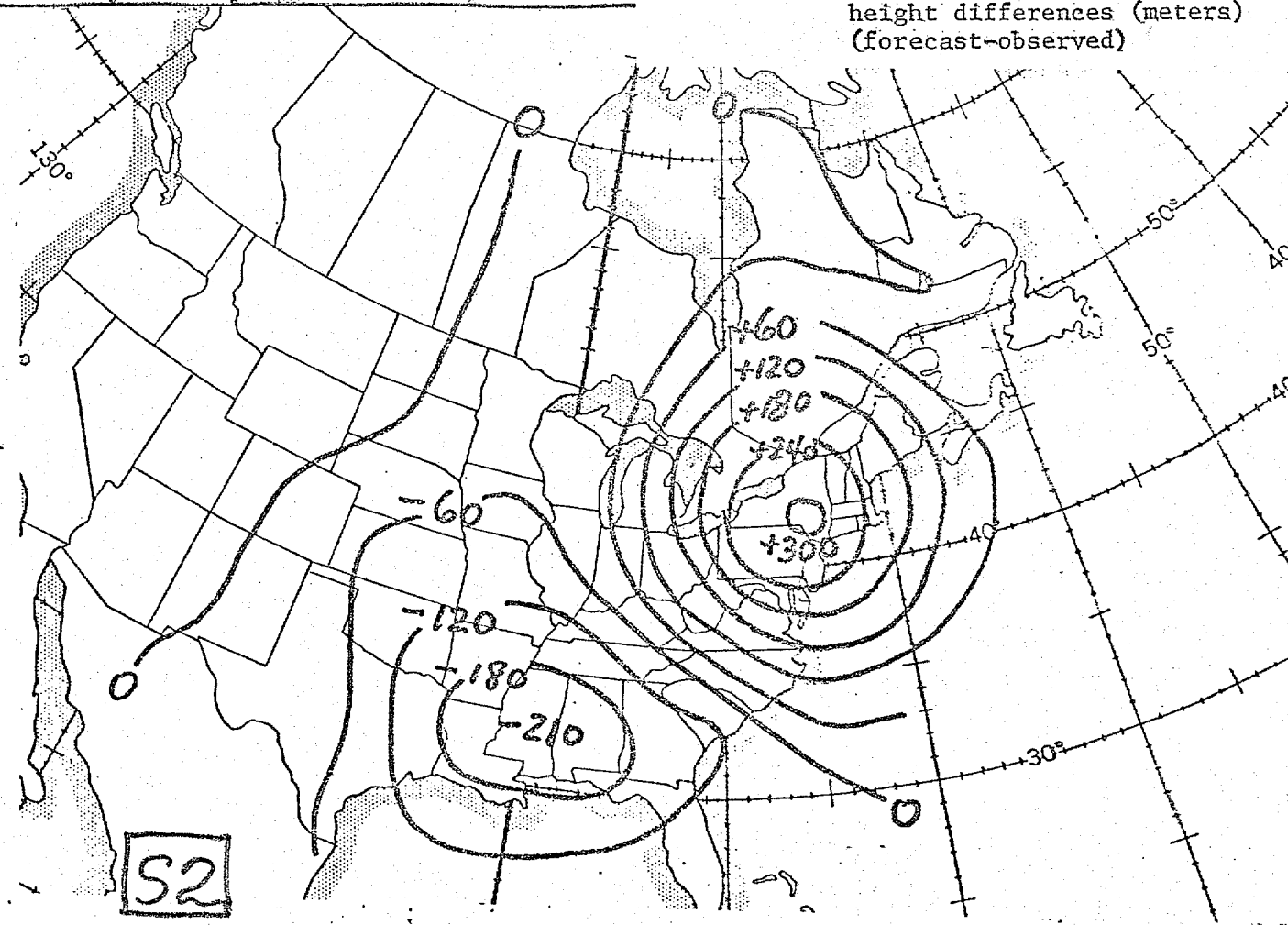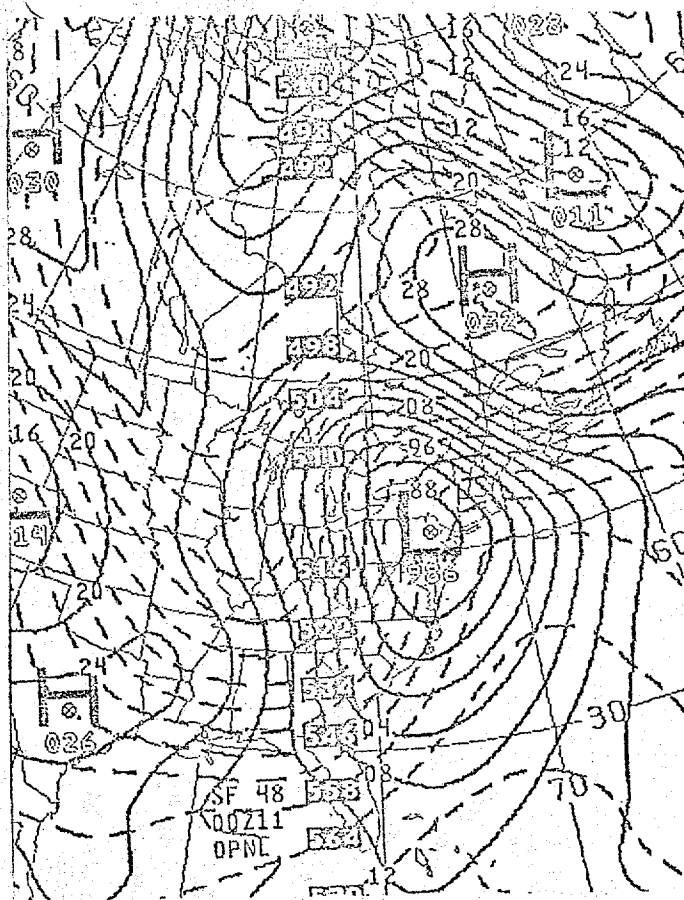
HFM   6L PE

48HR FCST   SFC/1000-500 THICKNESS VALID 00Z TUE 11 JAN 1977

HFM   Figure 6.   6L PE
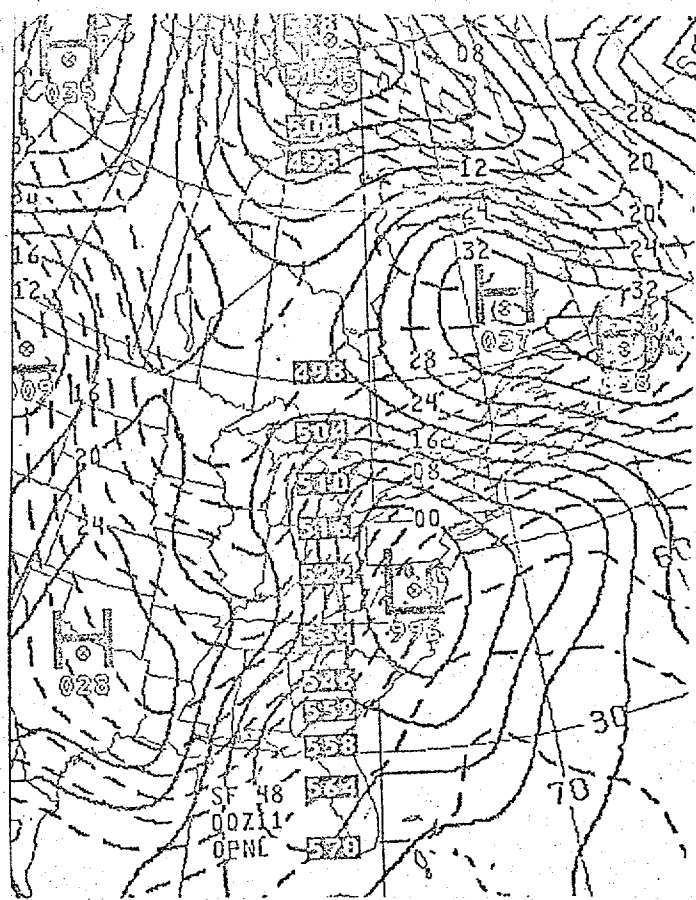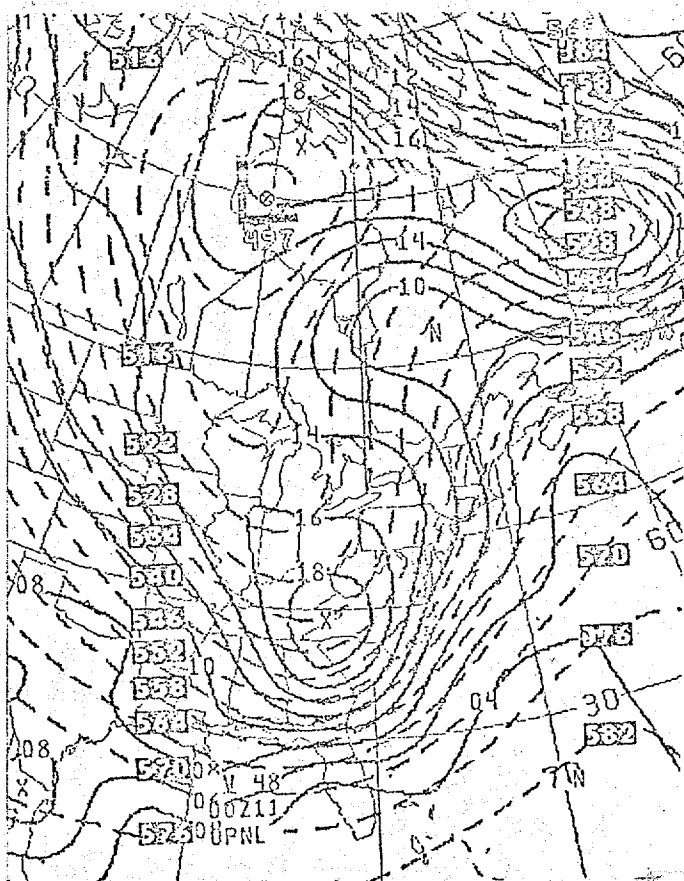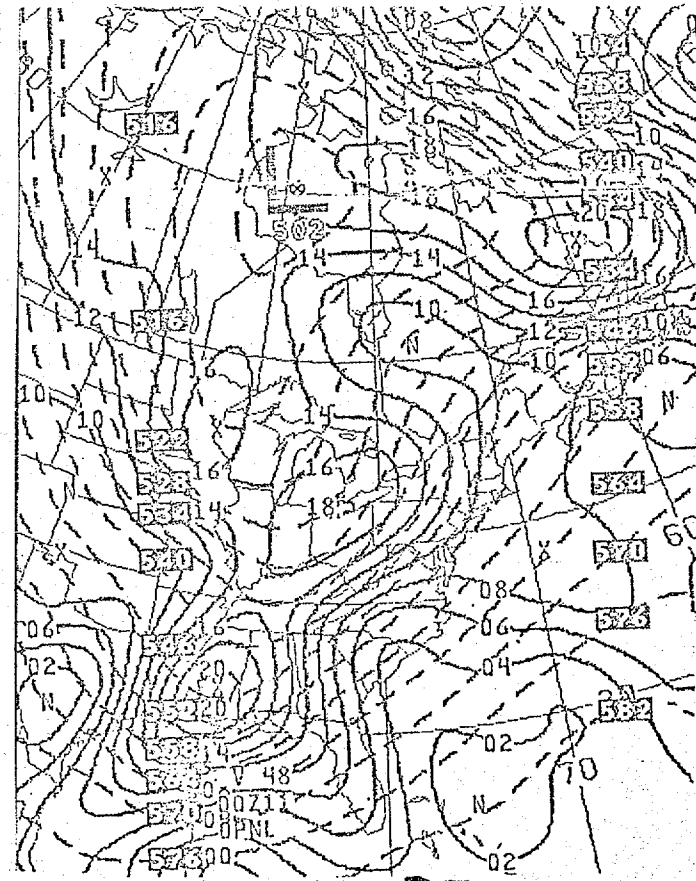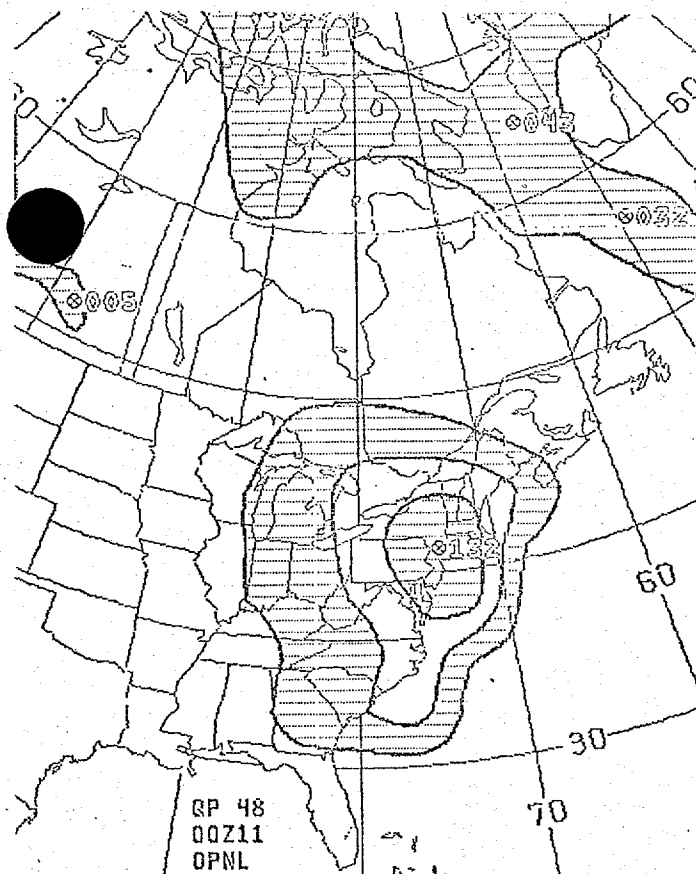
S4
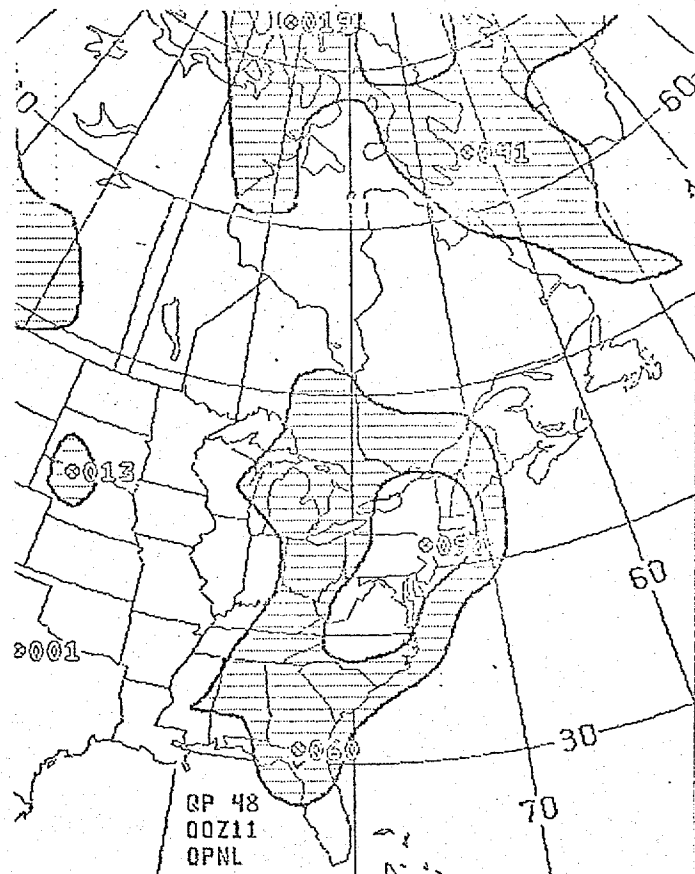
S2
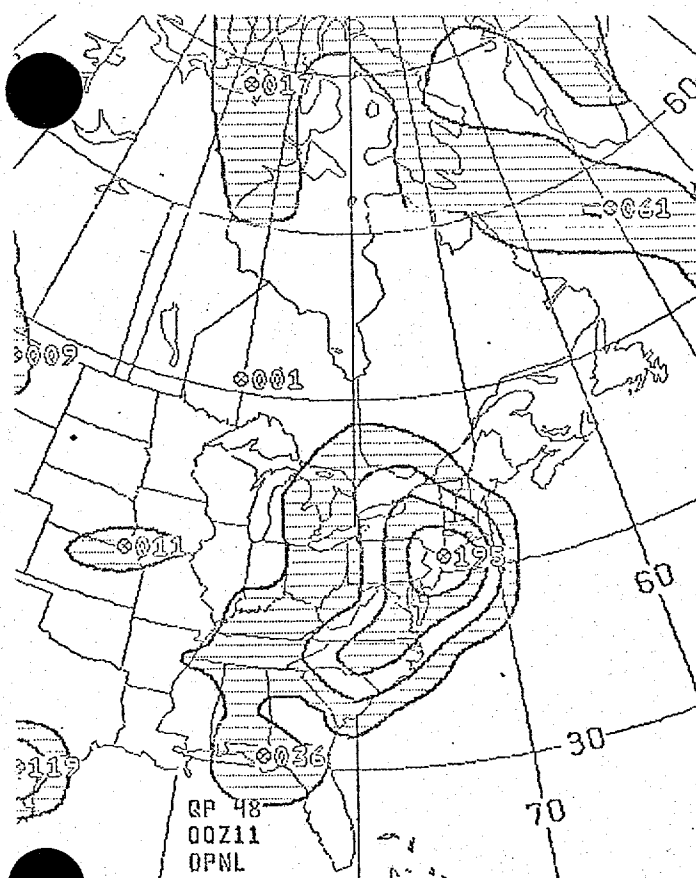
HFM
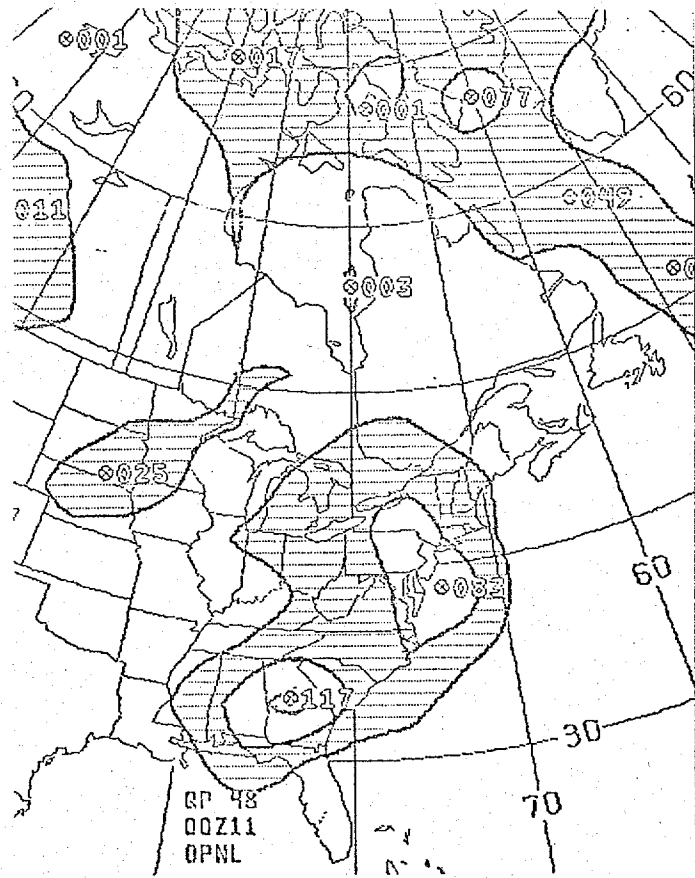
GL PE

Figure 7.

48HR FCST   SFC PRECIP. AMOUNT   VALID 00Z TUE 11 JAN 1977

Figure 8. Observed 12-hr precipitation amounts (inches) for the 36-48 hour forecast from 00Z 9 Jan 77.

VERIFICATION

HFM

S4

S2
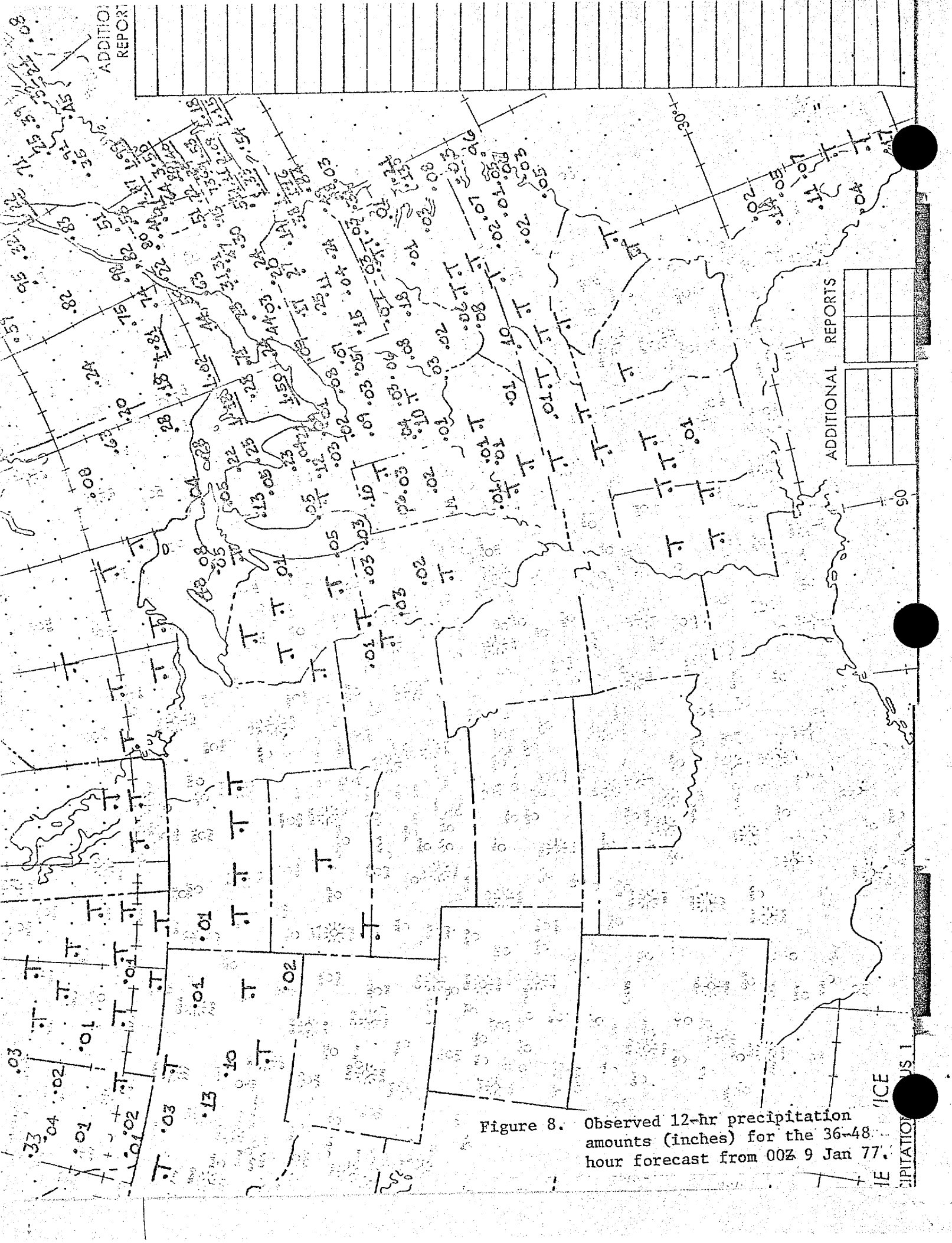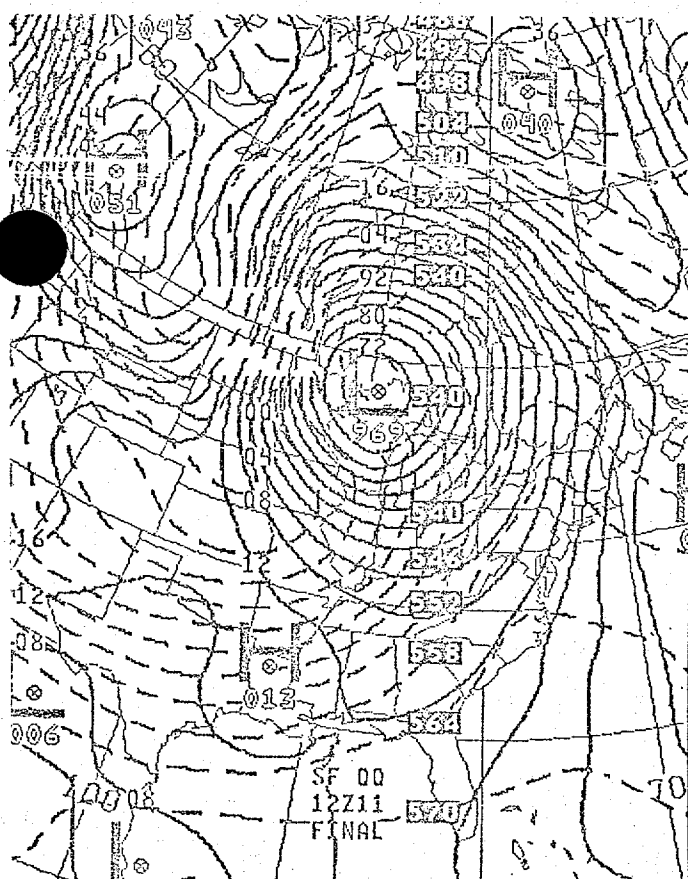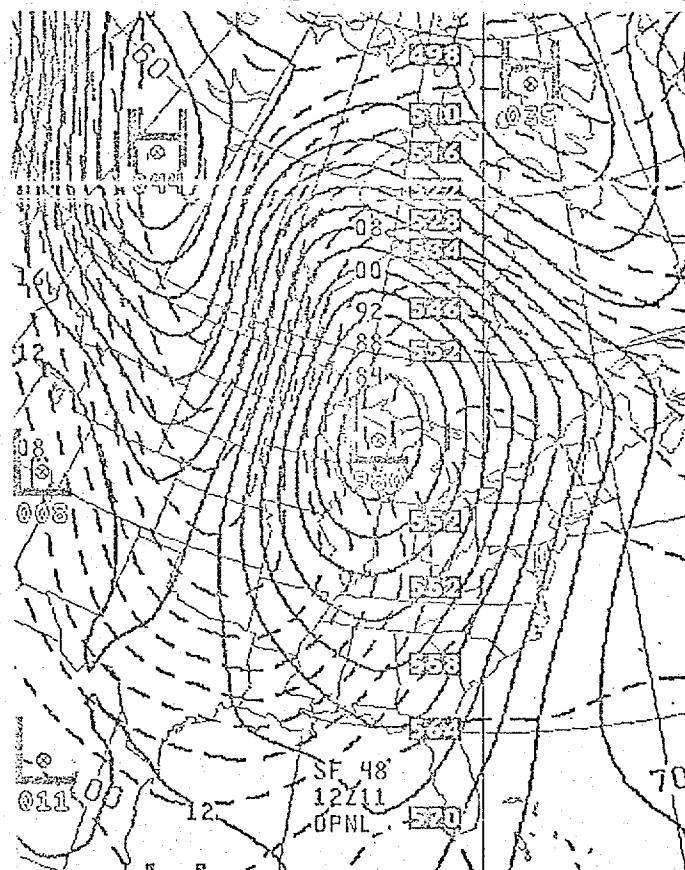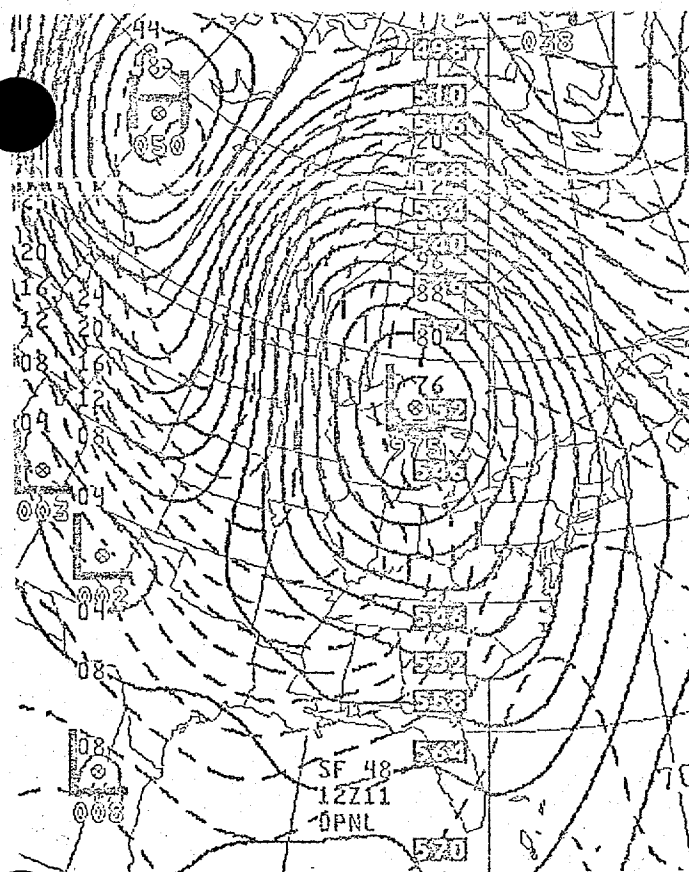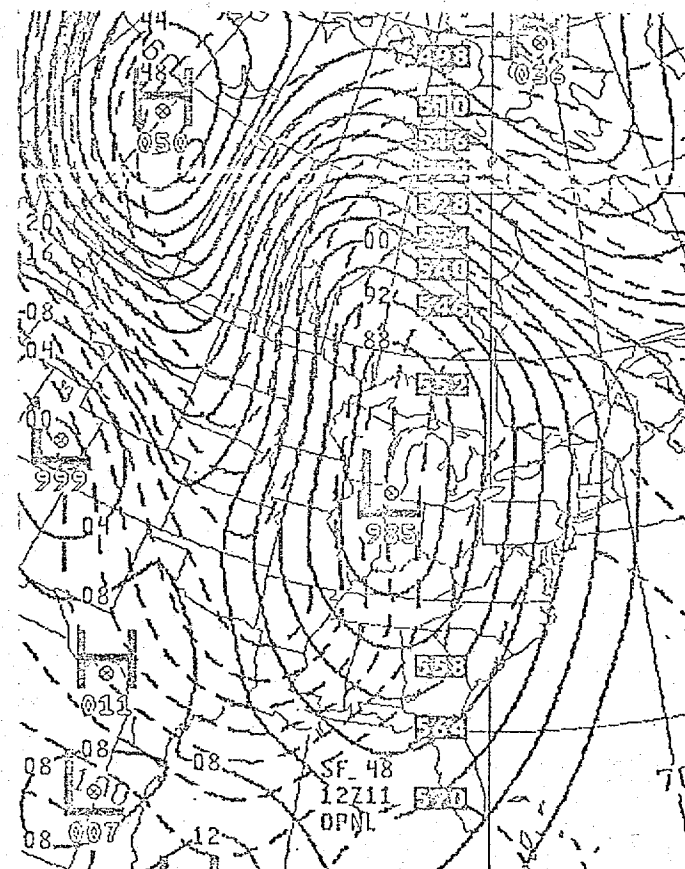
Figure 9

48HR FCST   SFC/1000-500 THICKNESS VALID 12Z SAT 11 JAN 1975

VERIFICATION

HFM

S4

Figure 10

S2
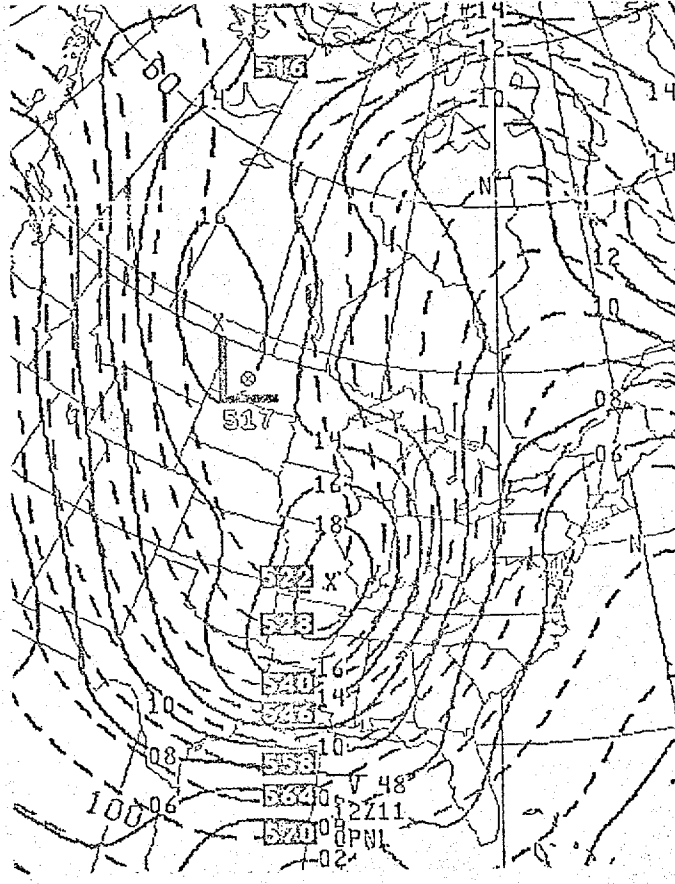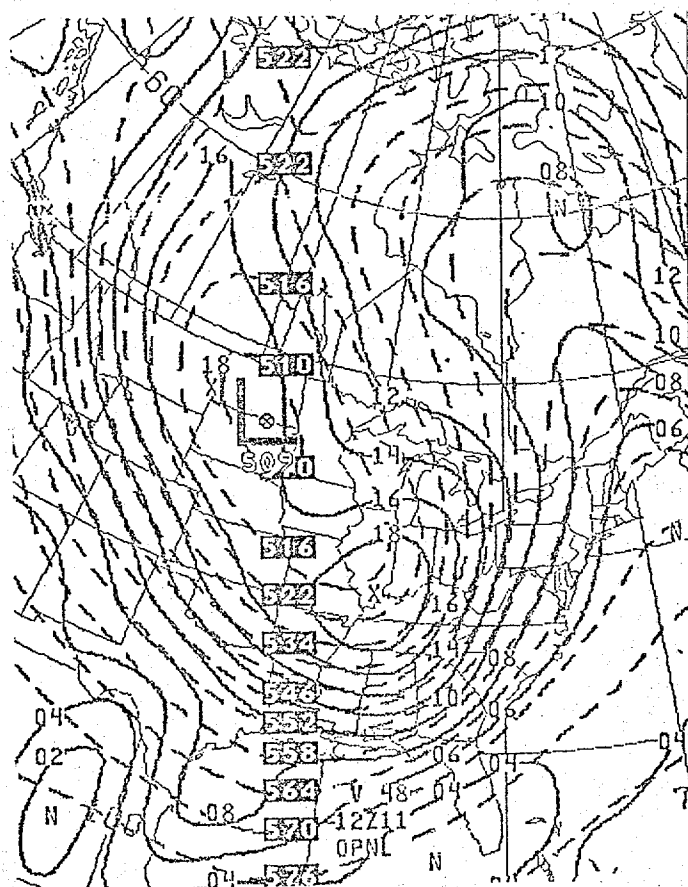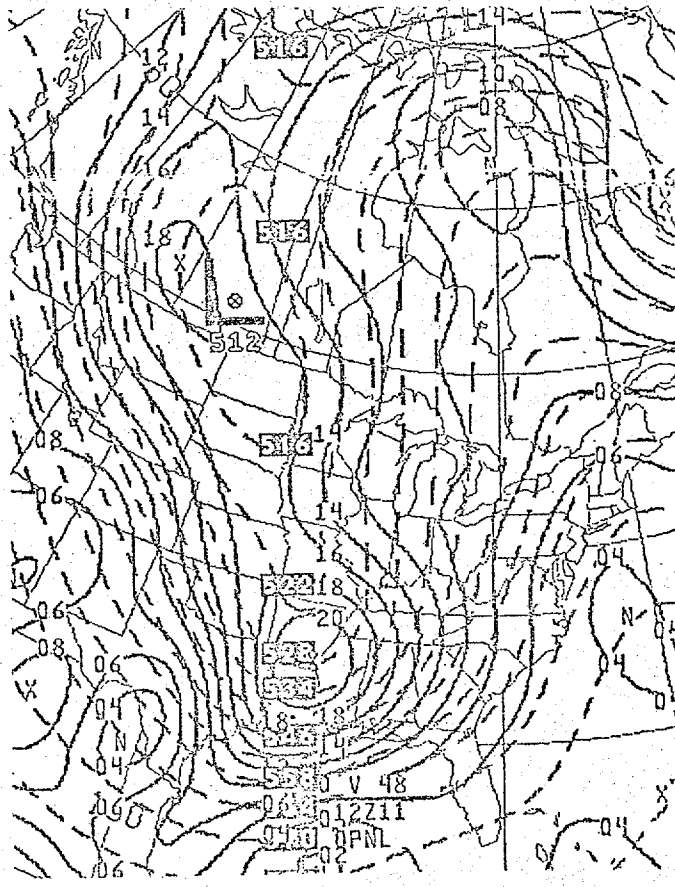
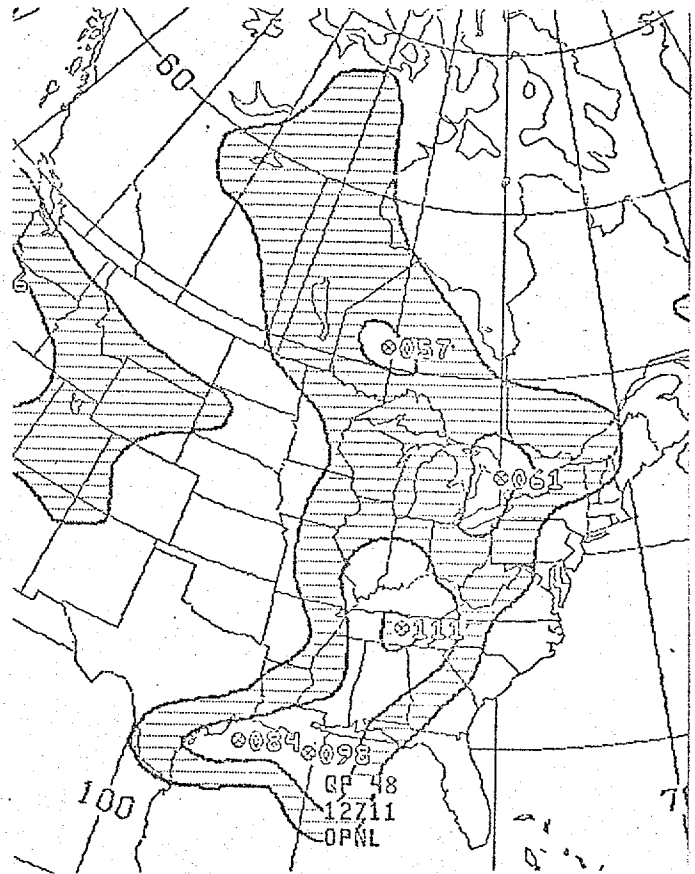48HR FCST 500MB   HEIGHTS/VORTICITY   VALID 12Z SAT 11 JAN 1975

VERIFICATION   HFM

S4   Figure 11   S2

48HR FCST   300MB   HEIGHTS/ISOTACHS   VALID 12Z SAT 11 JAN 1975
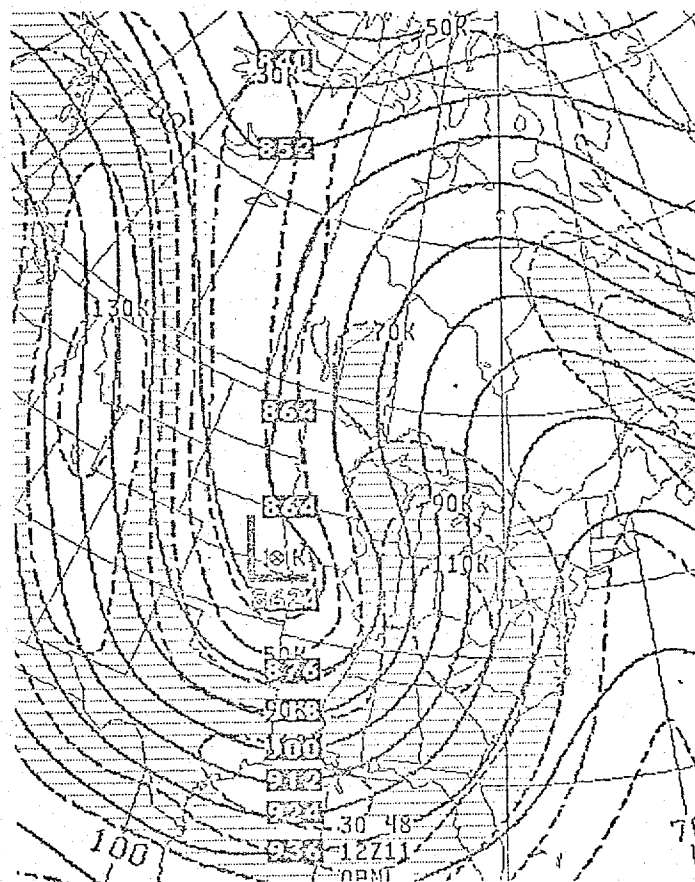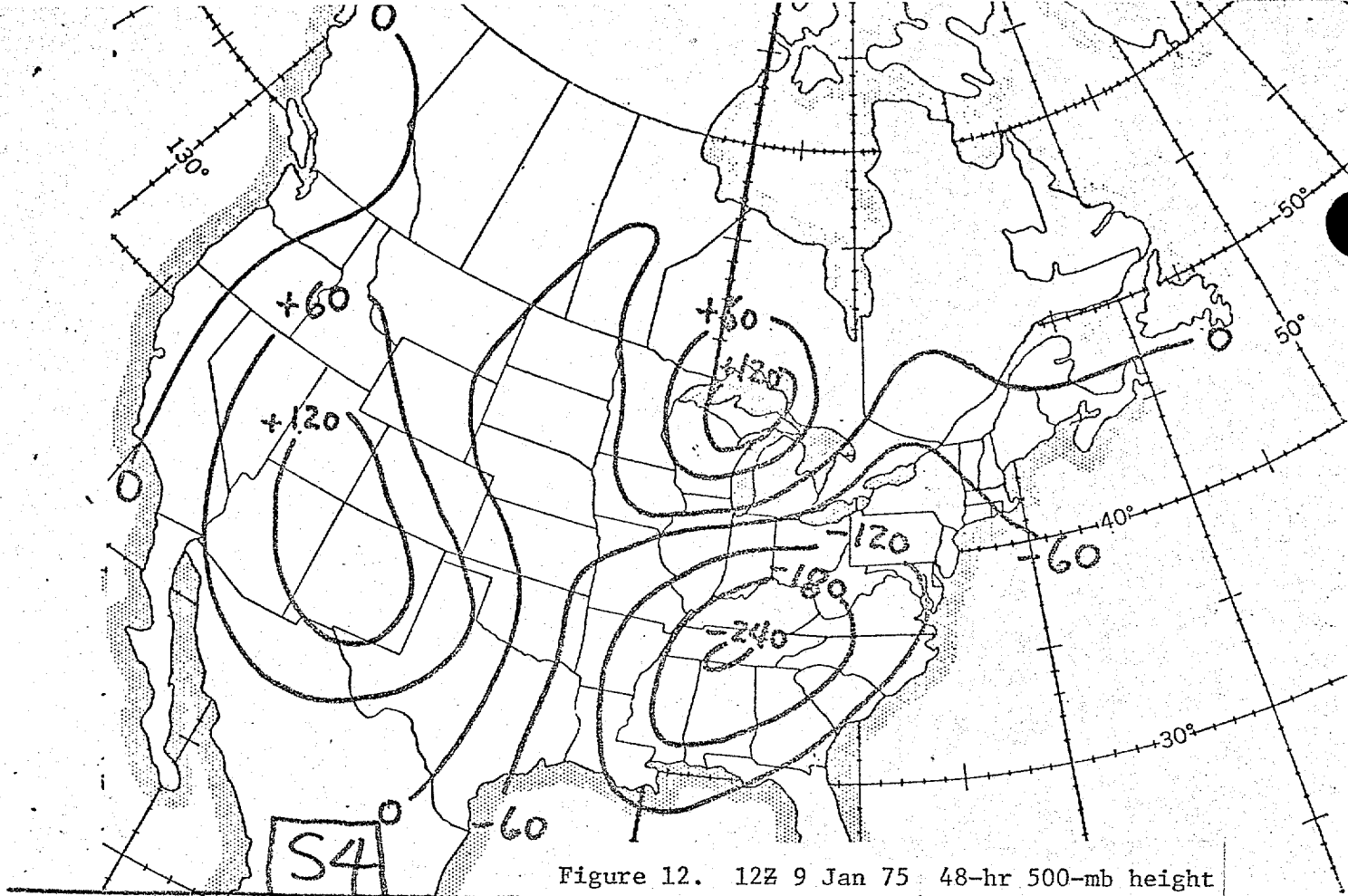
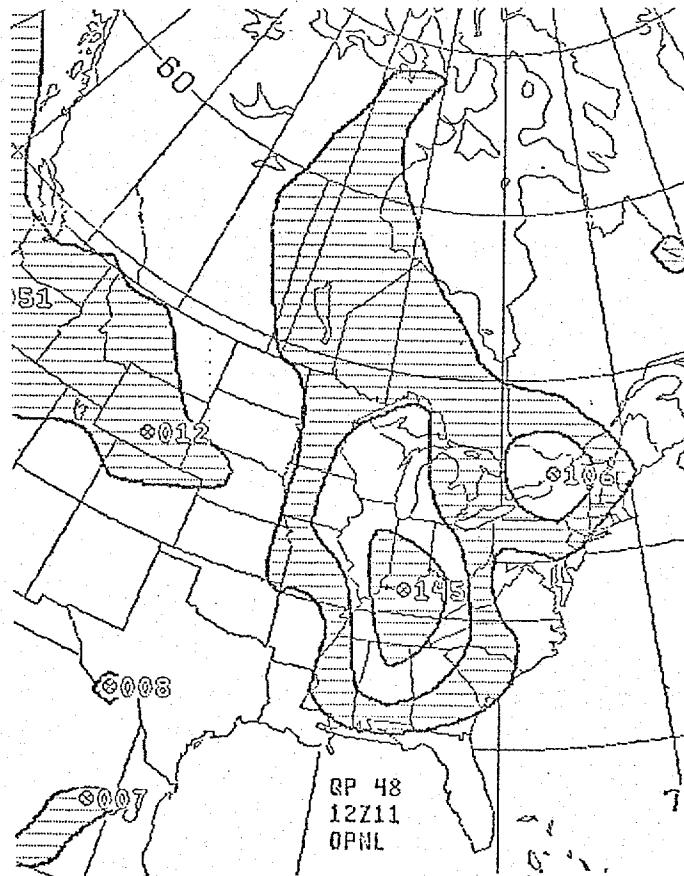Figure 12. 12Z 9 Jan 75 48-hr 500-mb height differences (meters) (forecast-observed)
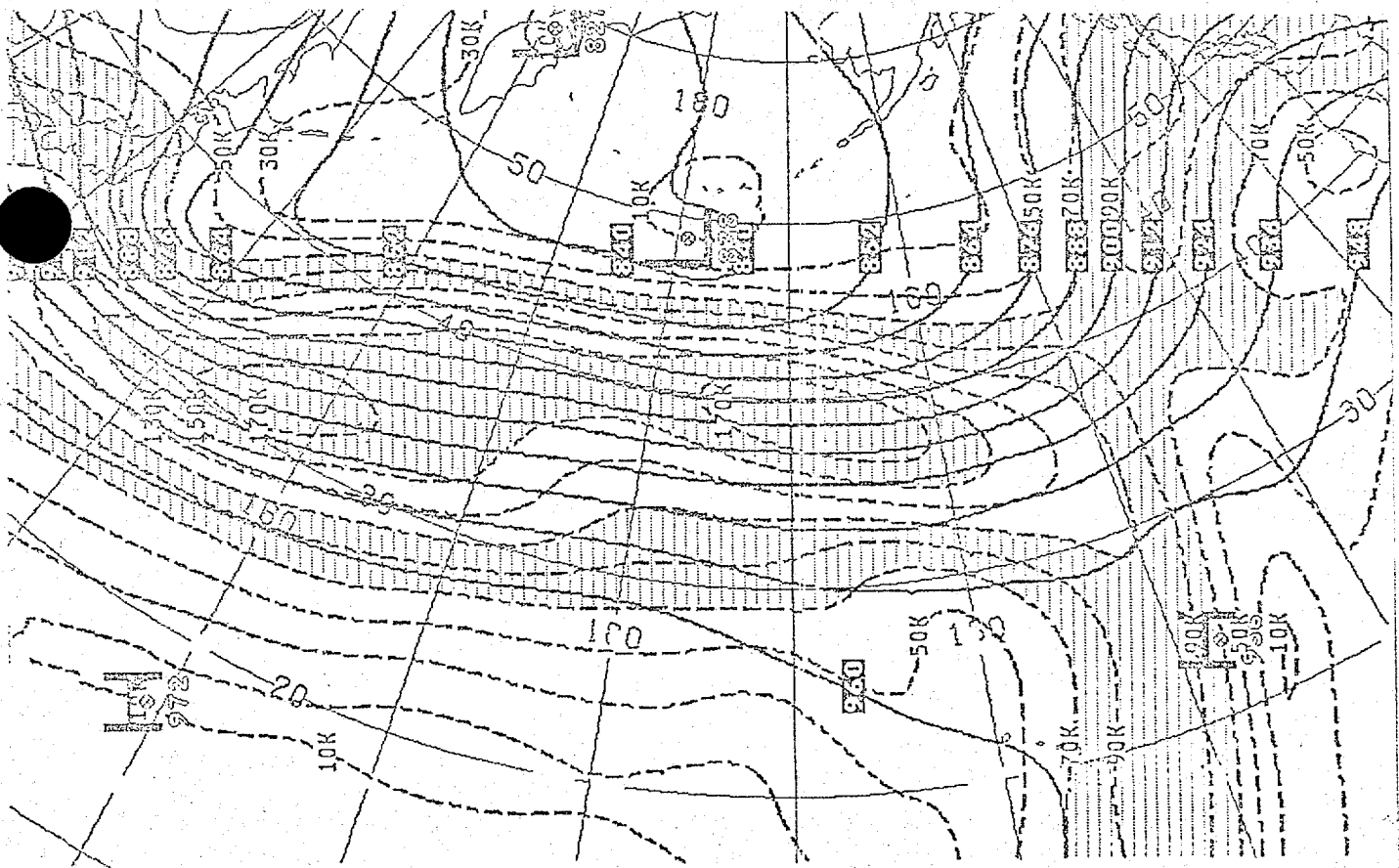
S4

S2

HFM

Figure 13

48HR FCST   SFC PRECIP. AMOUNT   VALID 12Z SAT 11 JAN 1975
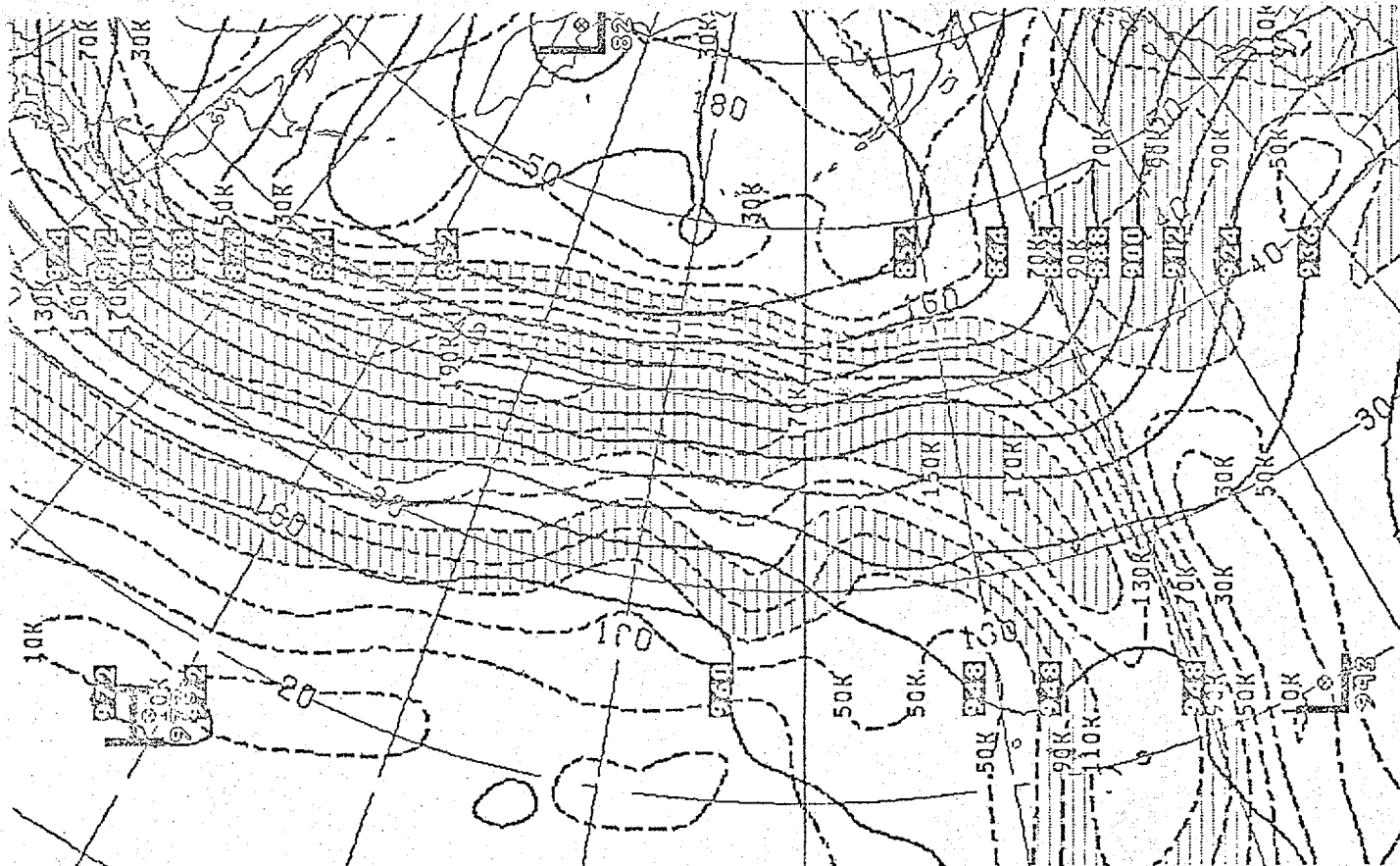
Figure 14. Observed 12-hr precipitation amounts (inches) for the 36-48 hr forecast from 12Z 9 Jan 75.

S2
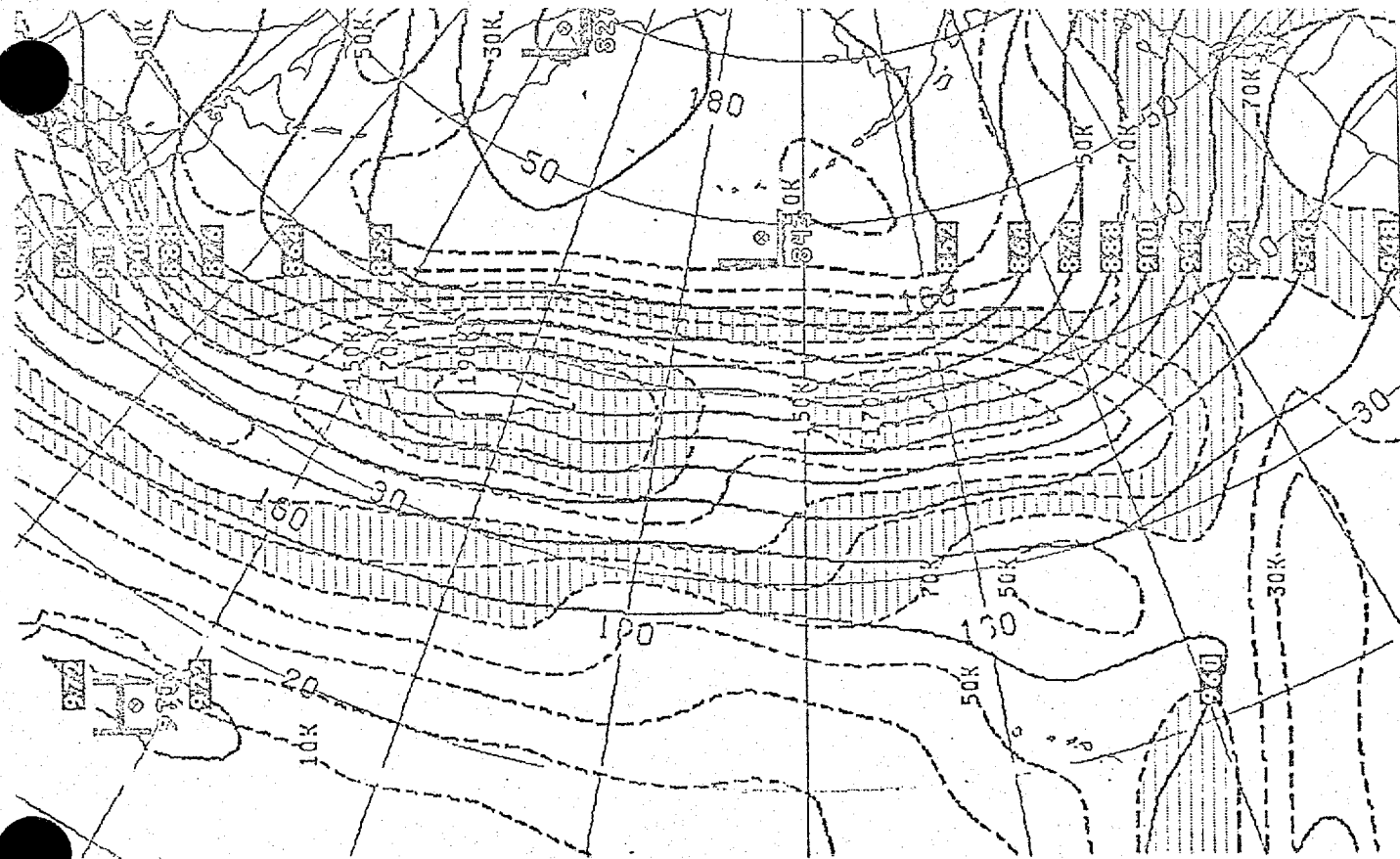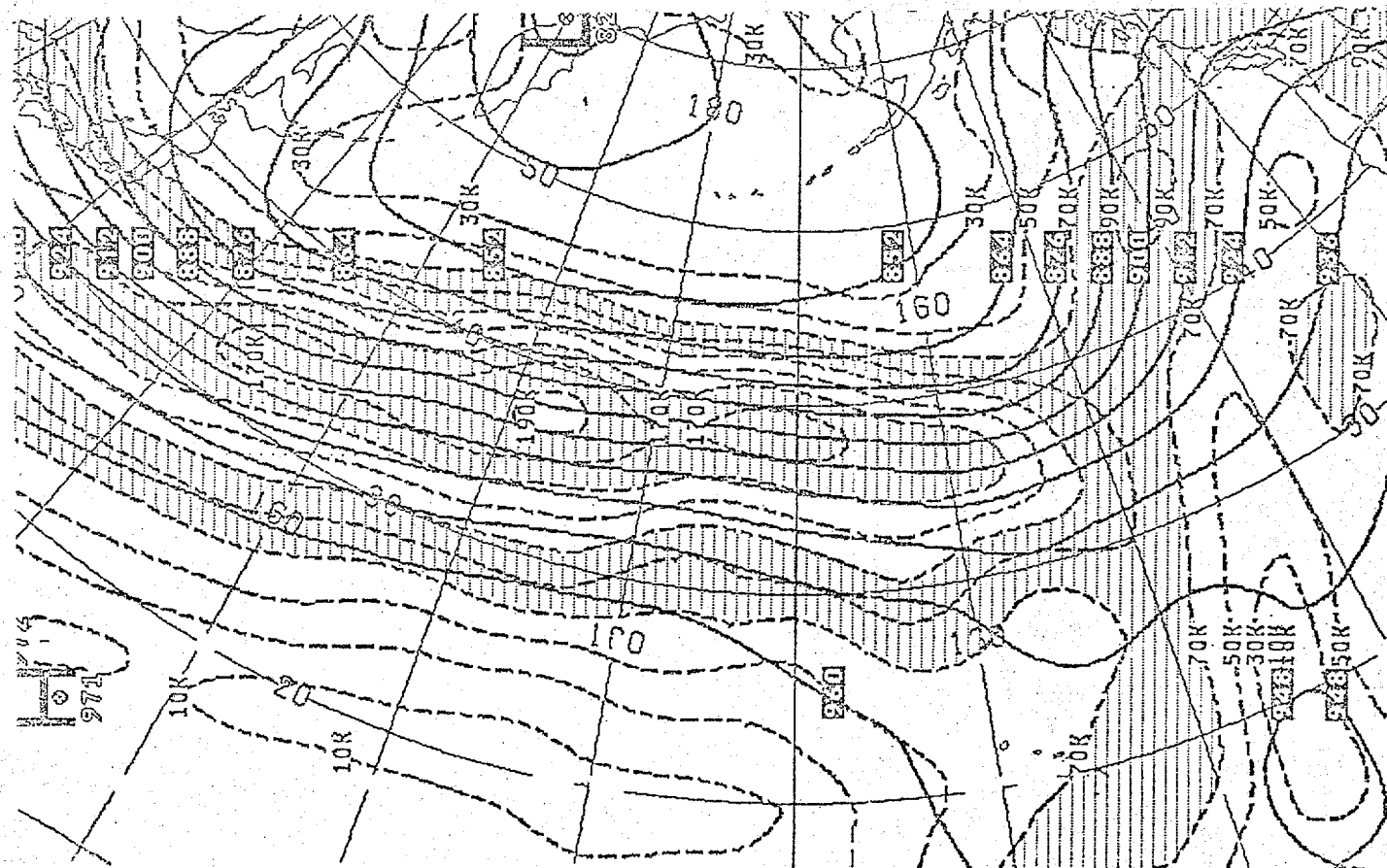
S4

Figure 15. 36-hr 300-mb heights and
wind speed 00Z 17 Feb 77.

6L PE

HFM Figure 16. 36-hr 300-mb heights and wind speed 00Z 17 Feb 77.

Figure 17. 300-mb verifying analysis
for the 36-hr forecast
made from 00Z 17 Feb 77.